Electronic Supplementary Material (ESI) for Journal of Materials Chemistry B.

Electronic Supplementary Information

Conjugation of gold nanoparticles with multidentate surfactants for enhanced stability and biological properties~~Multidentate surfactants improve stability and conjugation to inorganic nanoparticles~~

Rany Rotem[1,¶], Marco Giustra[1,¶], Federica Arrigoni[1], Jessica A. Bertolini[1], Stefania Garbujo[1], Maria A. Rizzuto[1], Lucia Salvioni[1], Linda Barbieri[1], Luca Bertini[1], Luca De Gioia[1], Miriam Colombo[1,], Davide Prosperi[1,*]*

[1] University of Milano Bicocca, Milan, Italy.

¶ These authors contributed equally.

* corresponding authors

1. Experimental design and expected results:

The experimental design and expected results for a surfactant that is irreversibly bound to the NPs is presented in figure 1S. Notably it shows an initial decrease in surfactant concentration in the precipitate (while most surfactant is unbound), and later a plateau (as most surfactant is bound to the NPs).

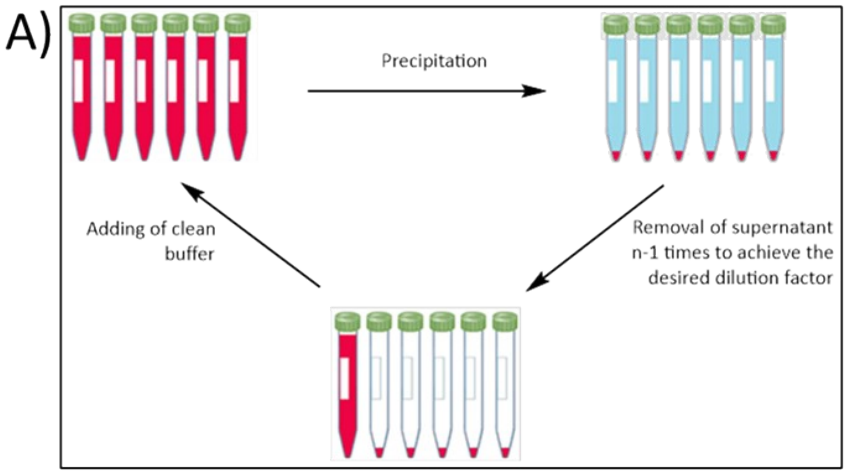

B)

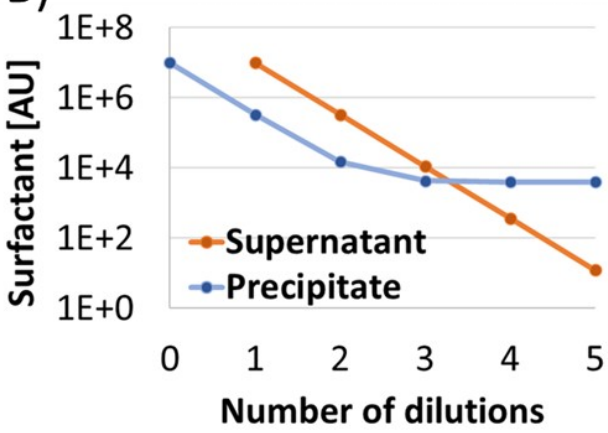

C)

# dilution	Dilution factor	SUP	NPs	Precipitate
0	1	10000000	4000	10004000
1	30	333333	4000	337333
2	900	11111	4000	15111
3	27000	370.4	4000	4370.4
4	810000	12.3	4000	4012.3
5	24300000	0.4	4000	4000.4

Figure 1S: A) experimental design, showing the sequence of the first round of precipitation. All tubes were precipitated the same number of times, but with different number of supernatant dilutions. B) Idealized data of NPs irreversibly bound to the surfactant. Numbers are of concentration in arbitrary units. C) The data presented in B.

2. NPs of different size and chemistry:

We tested the stability of 5 nm gold NPs stabilized by the same three surfactants (PEG-SH, PMDA, PCP). The smaller size of the NPs meant higher centrifugal accelerations were necessary for sedimentation, and that was found to destabilize the NP covered with PCP. Therefore, we used a different method for free surfactant removal – by filtration. To make a proper

comparison, PEG-SH NPs were subjected to the same treatment. PMDA however forms micelles that are too big to be removed by filtration, and so these NPs were removed by centrifugation, following previously established protocols.

When using filtration, all samples were filtered the same number of times, and in control samples the filtrate was recycled to re-dilute the concentrate (thus eliminating effects unrelated to surfactant removal).

The surfactant dilution factor in these cases is dictated by the initial and final volume of each filtration, and by the permeability of the filter to the surfactant – that was found to be lower than the permeability of the solvent. For this reason, the reported dilution factor is only approximated and should be seen as a relative indication of the progressive removal of the surfactant, rather than absolute.

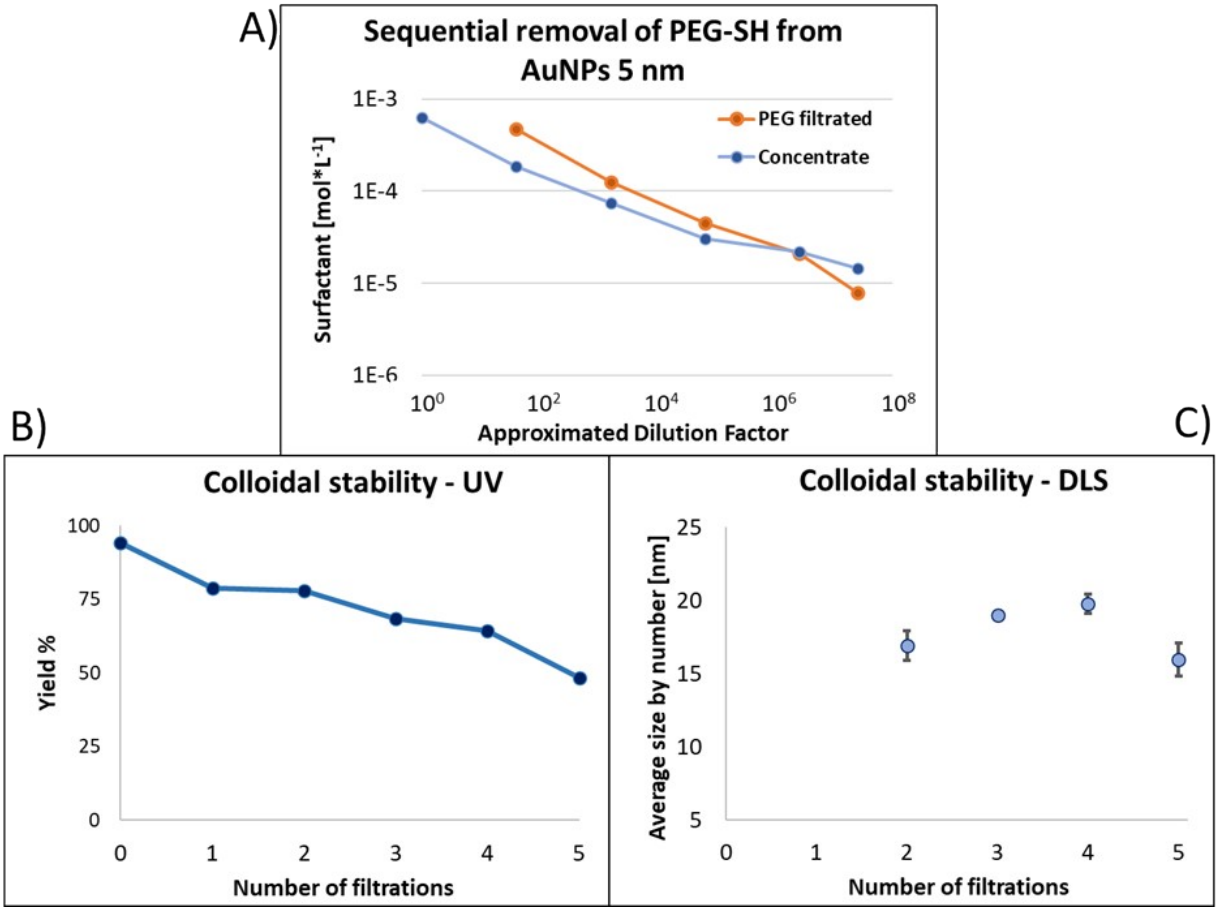

Figure 2S: 5 nm gold NPs stabilized with PEG-SH. As free ligand is removed the NPs are destabilized. Initial DLS measurements were limited by the high concentration of fluorescent surfactant, however an analogous non fluorescent sample had a hydrodynamic radius of 17.5 ±0.5 nm before removing the excess ligands (analogous to sample with 0 dilutions missing from the figure). Error bars represents 3 measurements of the same sample.

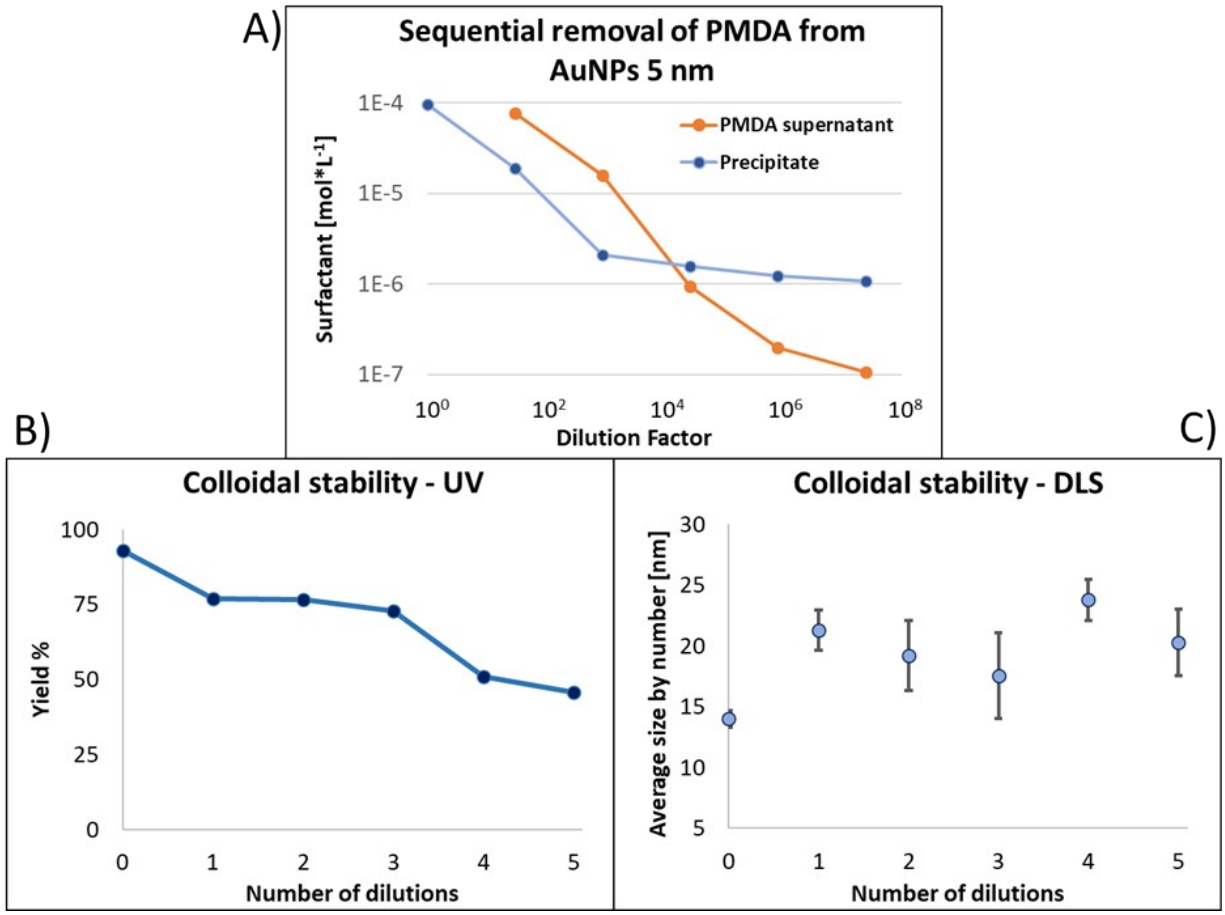

Figure 3S: 5 nm gold NPs stabilized by PMDA. As excess surfactant is removed the colloid is destabilized as evident by decreasing plasmon absorption and increasing hydrodynamic size. Error bars represents 3 measurements of the same sample.

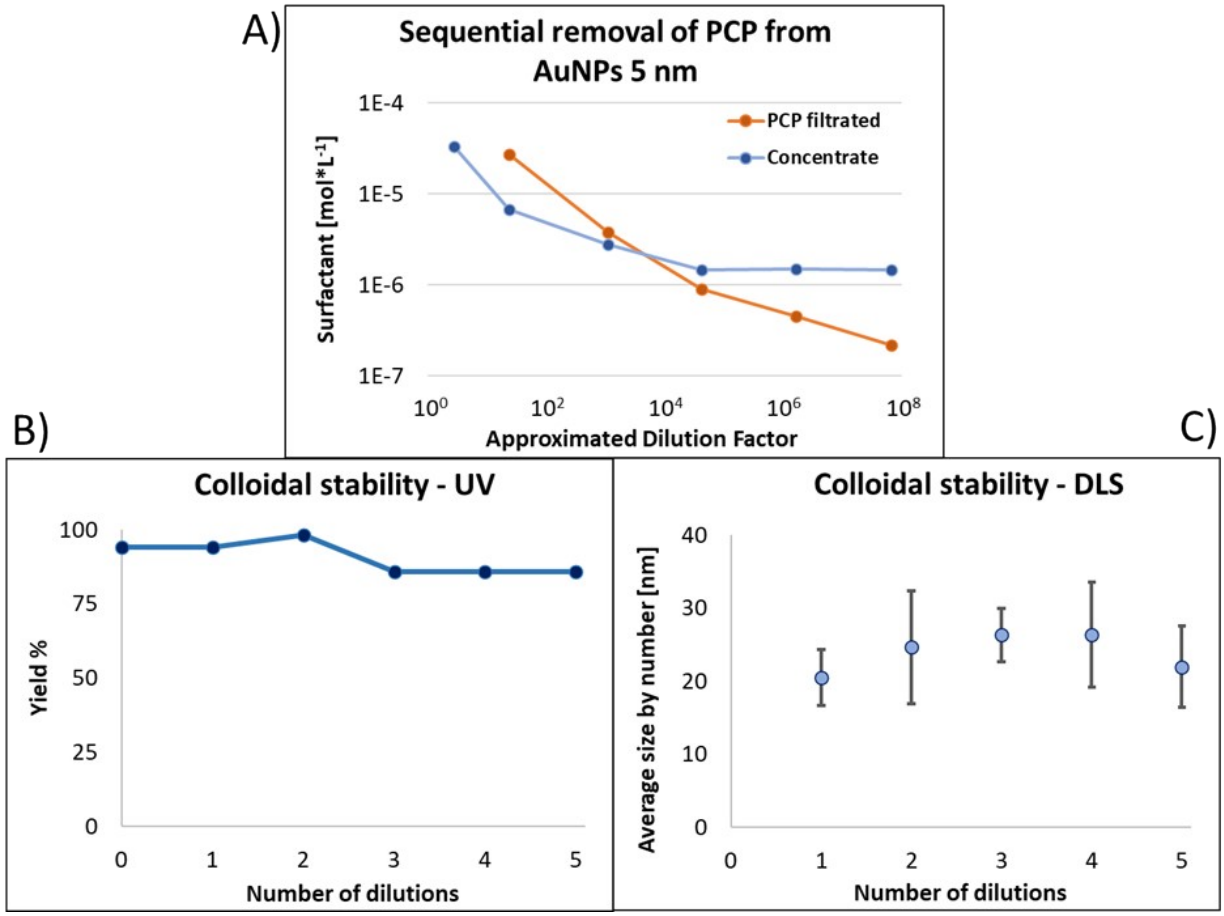

Figure 4S: 5 nm gold NPs stabilized by PCP maintain their stability as excess surfactant is removed. Also evident is a plateau of NPs emission (concentrate) in the last three washes, indicating the polymer stays bound to the NPs. Error bars represents 3 measurements of the same sample. DLS size of the first sample could not be measured due to excessive emission intensity of the sample.

To test this trend with NPs of different chemistry we used 50 nm iron oxide NPs. As surfactant we used the currently popular PMDA and a previously published multidentate polymer utilizing dopamine as iron oxide binding ligand (poly[isobutene alt maleic anhydride] grafted with both dopamine and 750 Da PEG named here PDP).

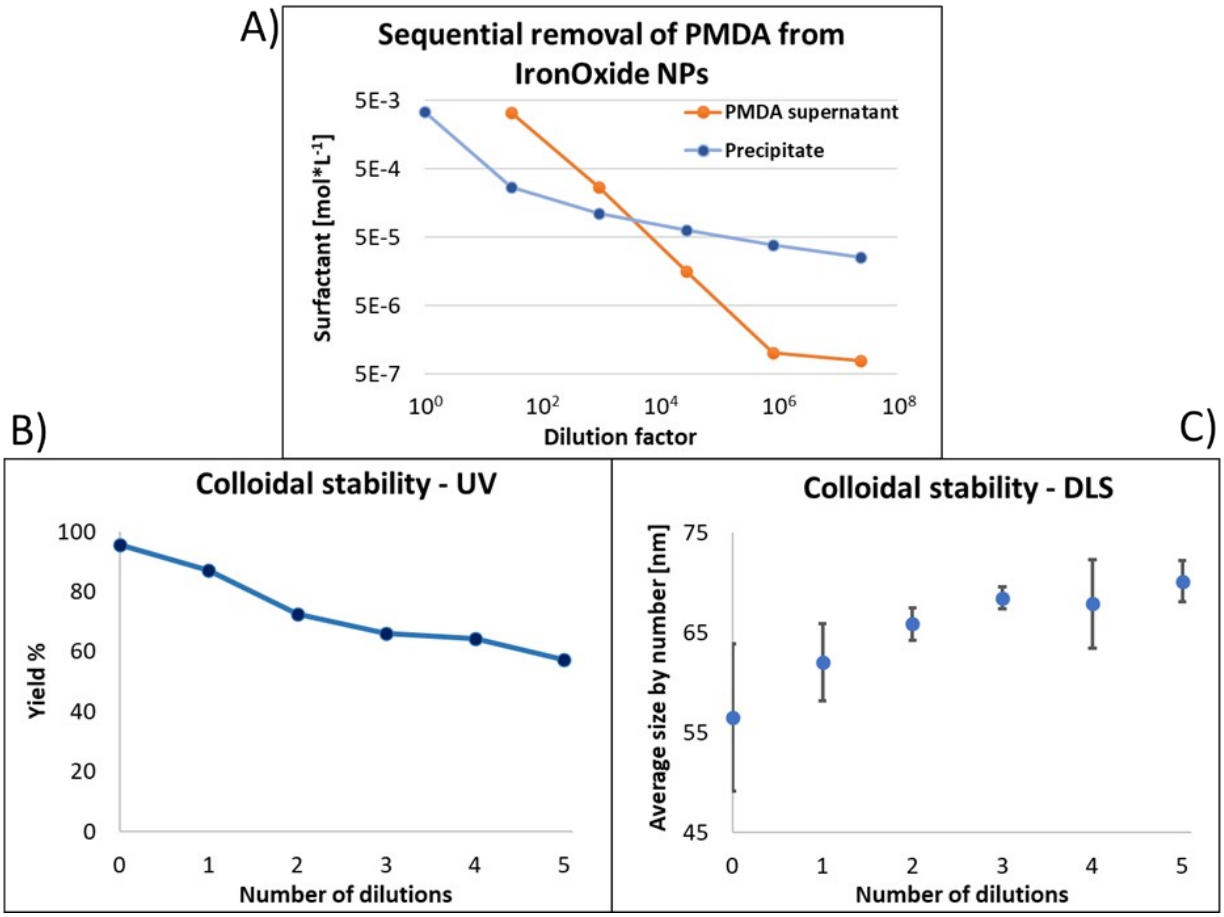

Figure 5S: 50 nm Iron Oxide NPs stabilized with PMDA. As excess surfactant is removed instability is evident by both loss of absorption and increased hydrodynamic size. Error bars represents 3 measurements of the same sample.

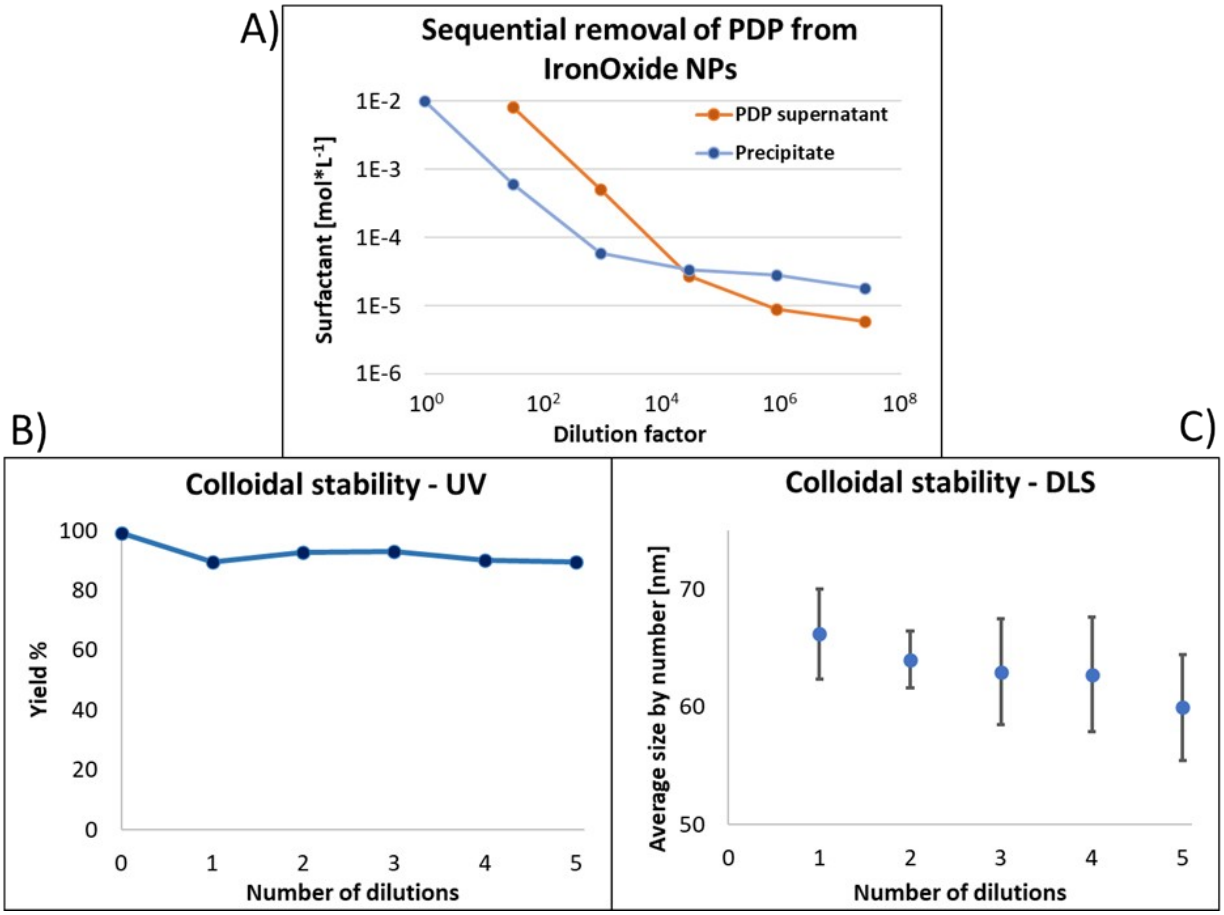

Figure 6S: 50 nm Iron Oxide NPs stabilized with PDP. Unlike with PCP, here a decrease in hydrodynamic diameter is evident, as well as a slow but continual loss of fluorescent intensity from the NPs (precipitate). Both might be evidence of surfactant loss from the NP's surface. Still, a very clear improvement in NP stability is evident by all parameters compared to PMDA (rate of emission loss during the last 3-4 precipitations, loss of absorption, and aggregation). Error bars represents 3 measurements of the same sample. DLS size of the first sample could not be measured due to excessive emission intensity of the sample.

3. Characterization of NPs

During NP preparation (in the case of PEG-SH and both PCP and PDP) and ligand exchange, the selective removal of the previous ligand, dodecylamine, was done through anti-solvent precipitation of the NPs with the new surfactant. This process was monitored using a fluorescent assay to quantify the washed dodecylamine. The washing solvent (2.5% $CHCl_3$ in pentane) was evaporated and washed dodecylamine redissolved in aqueous buffer and quantified using Fluorescamine. Figure 7S shows the calibration curve for dodecylamine (in water) and the calculated concentration in chloroform after consecutive washes.

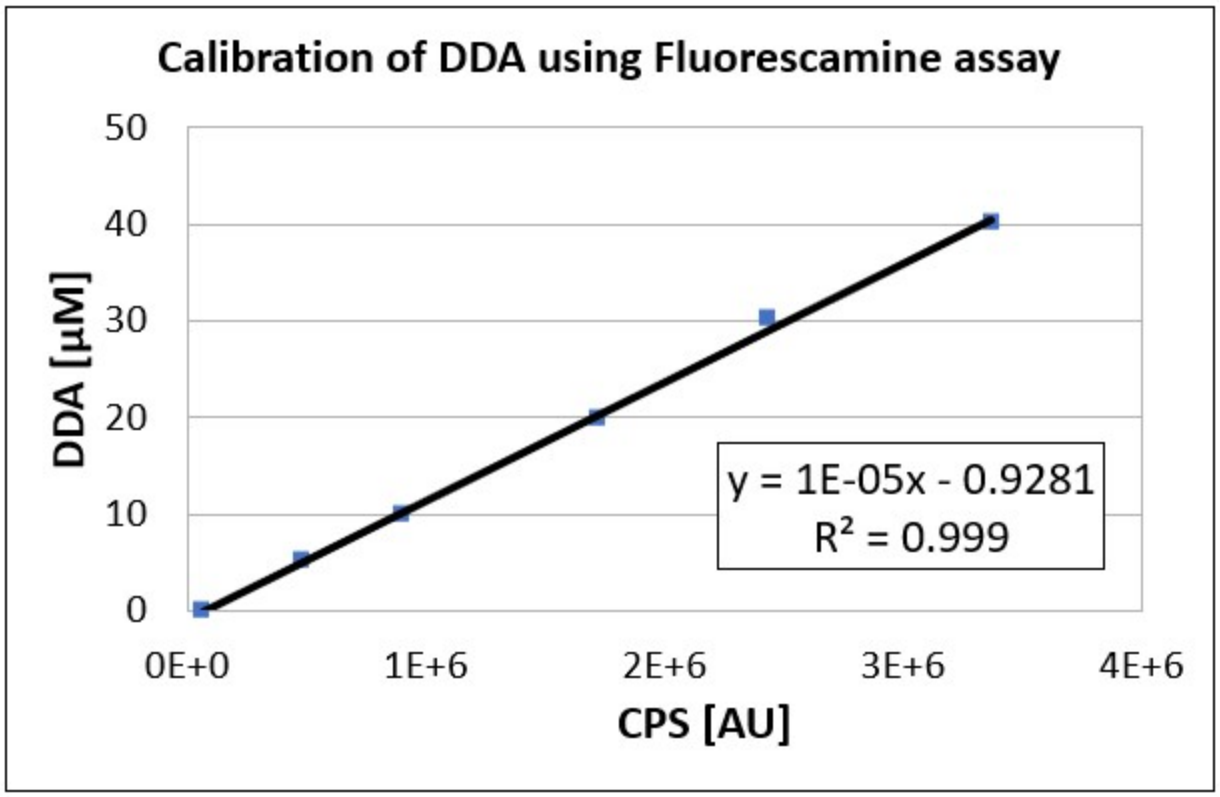

Number of Pentane Washings	DDA µM (in Chloroform)
1	2553.8
2	121.6
3	3

Figure 7S: DDA ligands were removed by antisolvent precipitation. The washed DDA was quantified using a pro-fluorophore. The table show the removed concentration from chloroform in each wash.

The utility of PCP was emphasized by demonstration of some basic protocols – blood plasma stability (figure 8S), lyophilization and re-solvation (figure 9S), protein conjugation such that most of the protein in solution is bound to the NPs (figure 10S) and NP cytotoxicity (figure 11S).

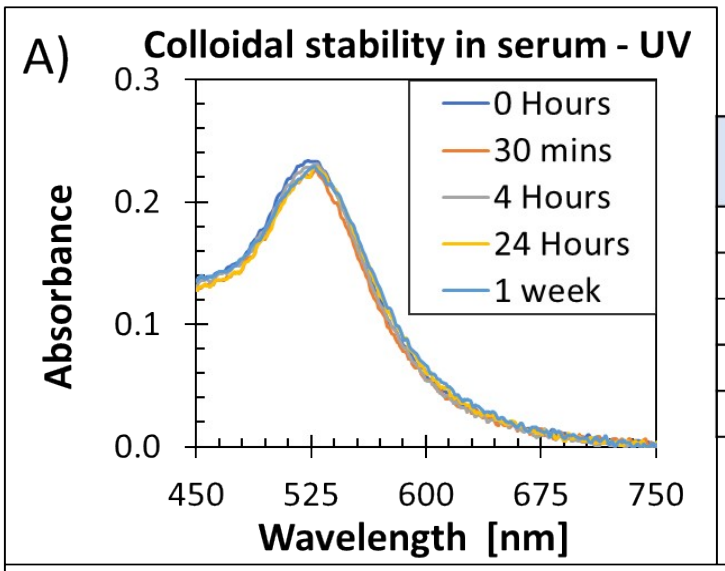

C)

Time (Hours)	Size distribution (nm)
No medium	19 ± 1
0.5	23 ± 2
4	29.7 ± 0.4
24	34 ± 4
168	37 ± 4

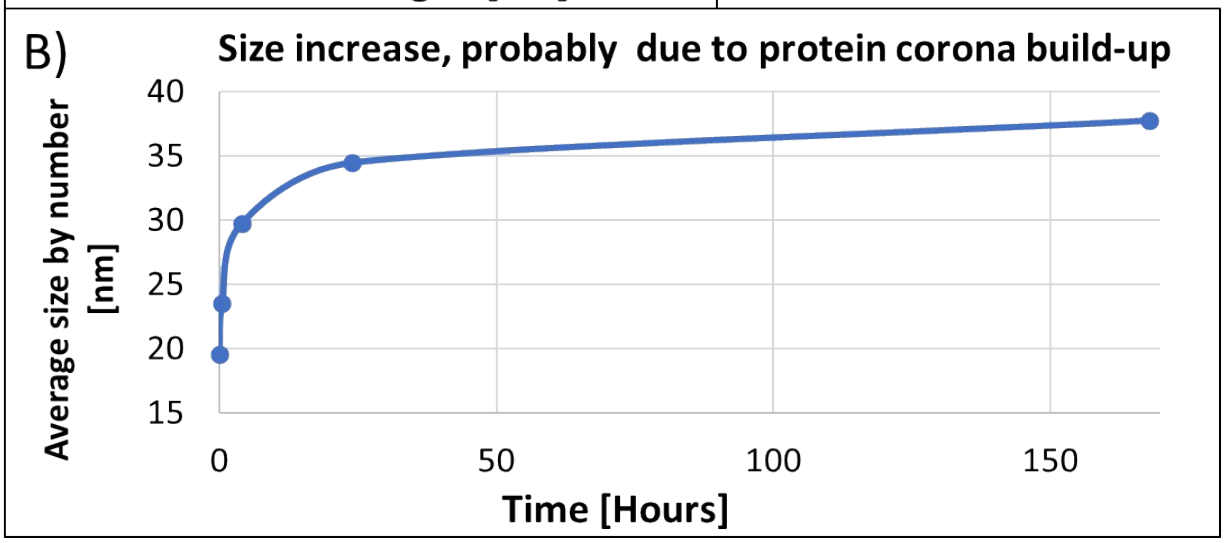

Figure 8S: the stability of 15 nm gold NPs was tested in DMEM with 10% plasma and 1% Penicillin-Streptomycin. A) showing no change in absorbance indicating high colloidal stability. B) showing increasing hydrodynamic size, probably indicating the buildup of a protein corona. C) showing the data from graph B)

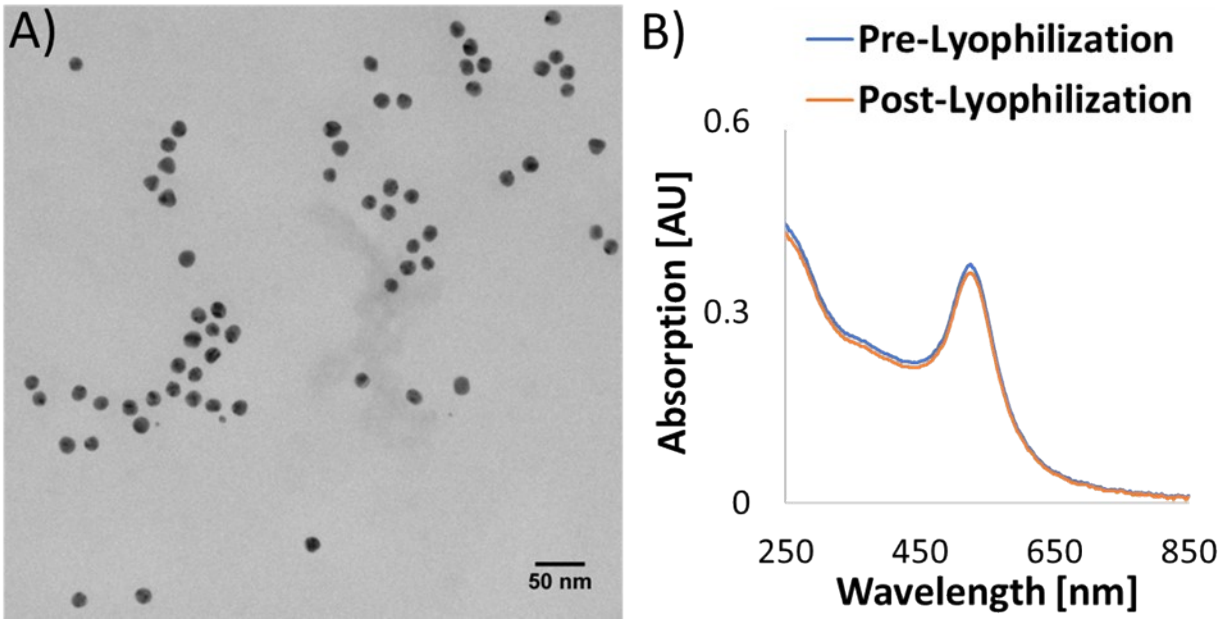

Figure 9S: A) TEM image of 15 nm gold NPs covered by PCP post lyophilized and re-dispersion in water. B) optical absorption of the same NPs, before and after lyophilization. The hydrodynamic diameter before and after was 18±1 and 19.6±0.8 nm. These characterization methods together indicate the NPs maintain their characteristics through lyophilization and re-dispersion.

	Conjugates [CPS]	Supernatant [CPS]	BSA bound [µg*mL^{-1}]	BSA free [µg*mL^{-1}]	BSA ratio
Value	2.12E+05	4.00E+04	0.175	0.032	5.6
Dev. St	0.07E+05	0.10E+04	0.006	0.007	1.0

	NPs yield [%]	NPs concentration [M]	BSA concentration [M]	BSA/NP
Value	91.2	3.63E-10	2.13E-09	6.0
Dev. St	3.7	0.12E-10	0.05E-09	0.2

Figure 10S: Characterization of protein-NP conjugates. 15 nm gold NPs stabilized with PCP were conjugated to BSA and purified such that the majority of the protein in solution is bound to the NP, while maintaining ~90% of the NPs at the end of the preparation/purification. Similar results were obtained with IgG conjugation.

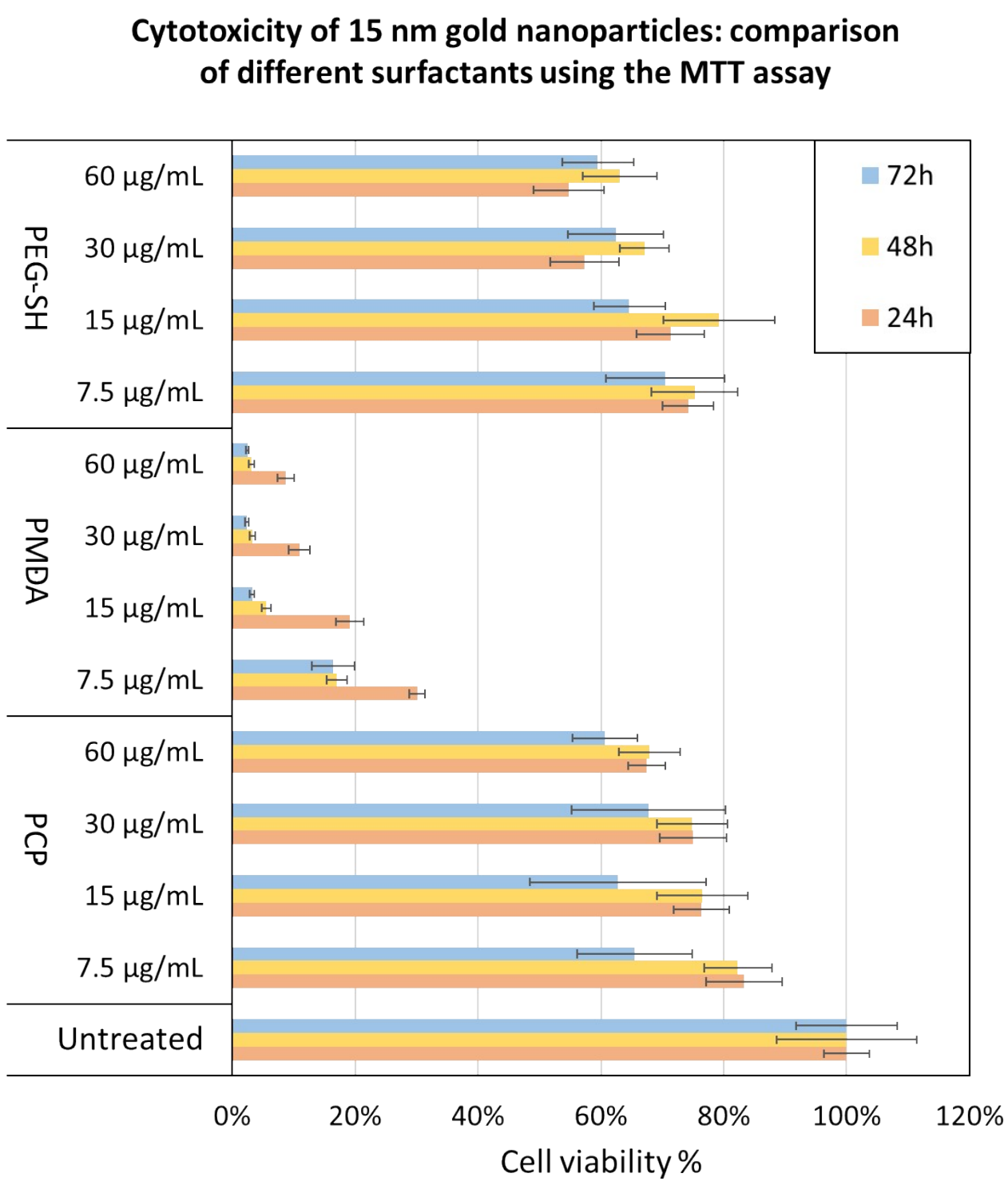
Cytotoxicity of 15 nm gold nanoparticles: comparison of different surfactants using the MTT assay
72h
48h
24h
PEG-SH
60 µg/mL
30 µg/mL
15 µg/mL
7.5 µg/mL
PMDA
60 µg/mL
30 µg/mL
15 µg/mL
7.5 µg/mL
PCP
60 µg/mL
30 µg/mL
15 µg/mL
7.5 µg/mL
Untreated
0%
20%
40%
60%
80%
100%
120%
Cell viability %

4. ~~*Figure 11S: MTT assay to compare the toxicity of gold NPs stabilized by different surfactant – PMDA and PEH-SH with polymer excess, and PCP without polymer excess. We choose this comparison due to our conclusion that it is not practical to use PMDA and PEG-SH without excess surfactant. Test was done using HeLa cells. The values are the mean of three different experiments in quadruplicates each. All samples are relative to the untreated cells, which are set as 100%. Error bars represents standard deviation.*~~

4. TEM imaging

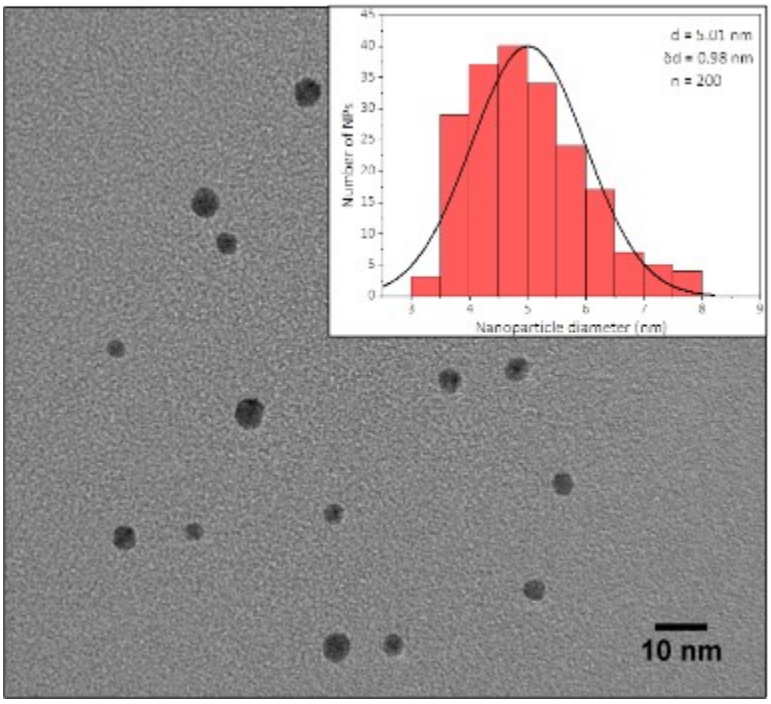

Figure 1~~2~~1S: 5 nm gold NPs stabilized by PMDA

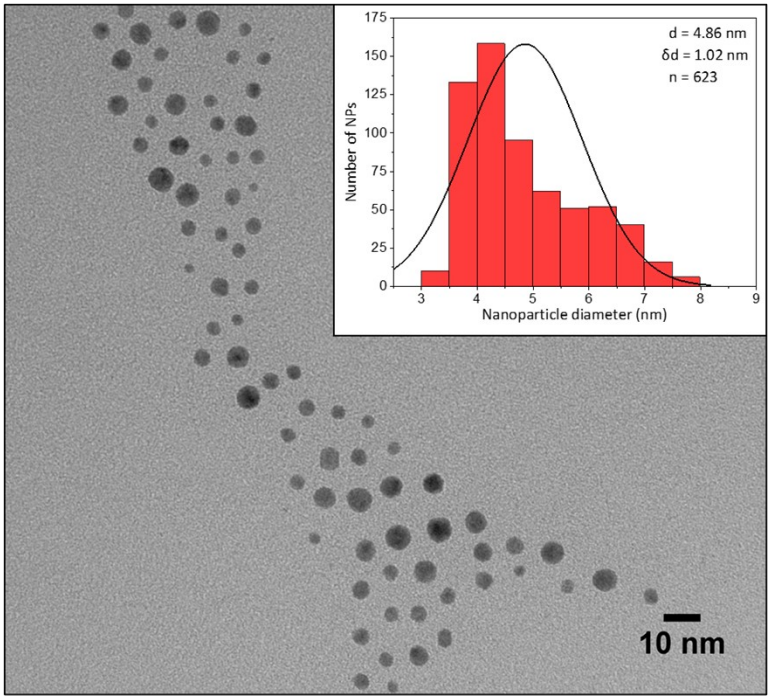

Figure 1~~2~~3S: 5 nm gold NPs stabilized by PEG-SH 2 kDa

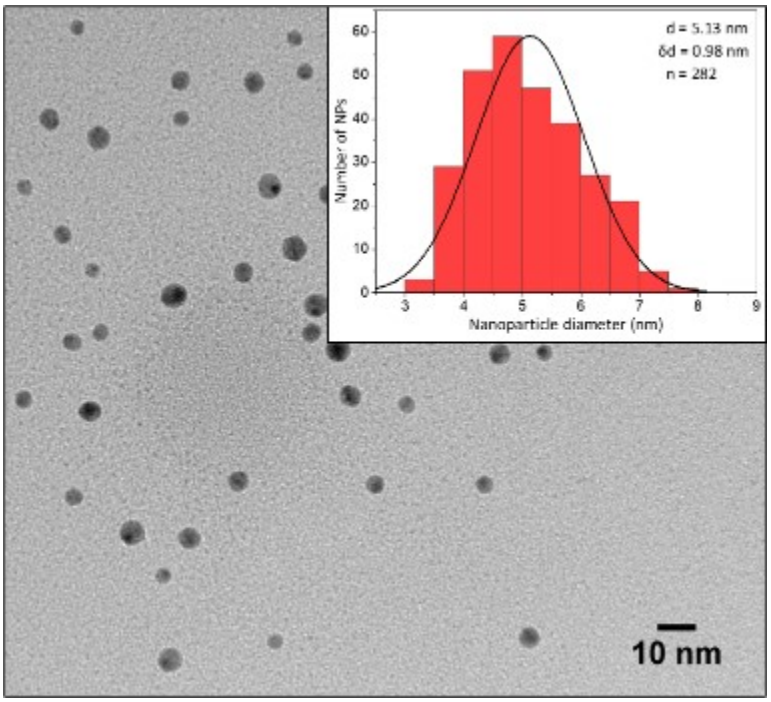

Figure 1~~3~~4S: 5 nm gold NPs stabilized by PCP

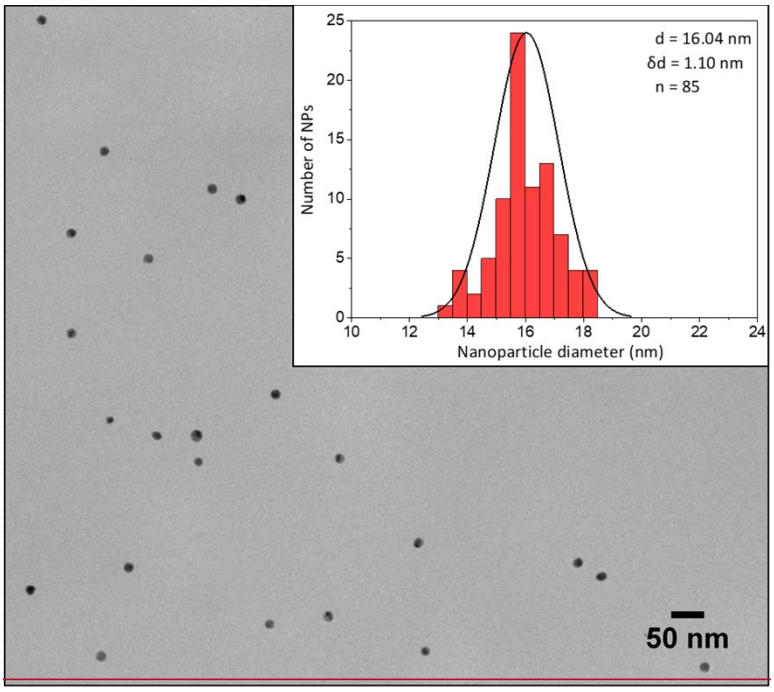

Figure 15S: 15 nm gold NPs stabilized by PMDA

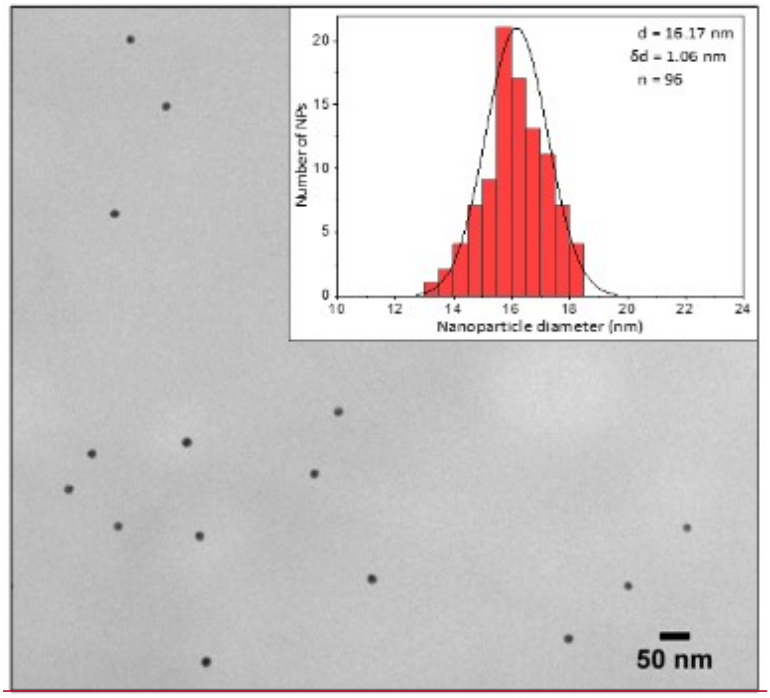

Figure 16S: 15 nm gold NPs stabilized by 2 kDa PEG-SH

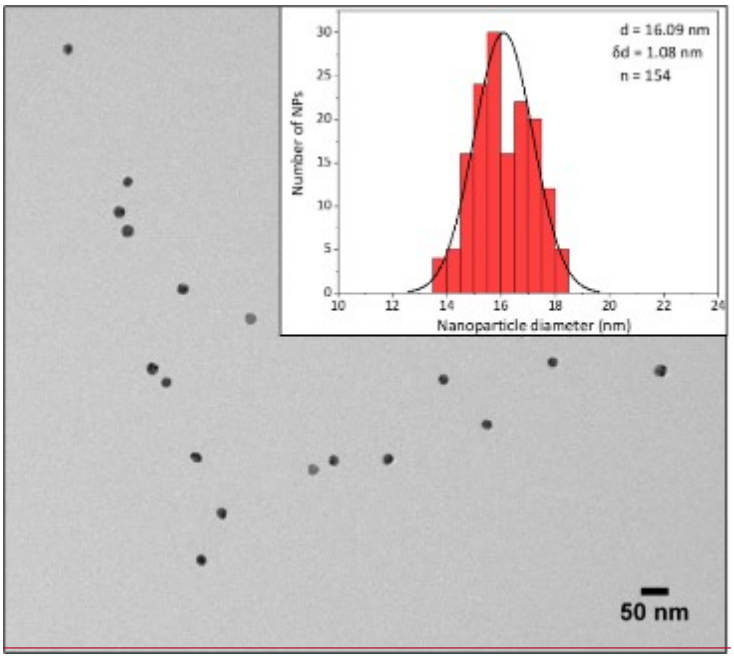

~~*Figure 17S: 15 nm gold NPs stabilized by PCP*~~

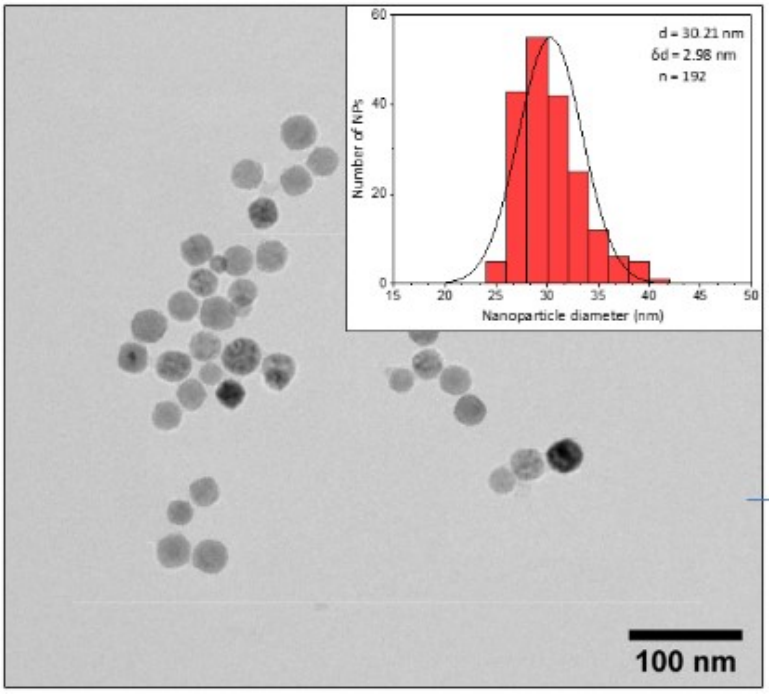

Figure 14~~18~~S: Iron Oxide NPs stabilized by PDP

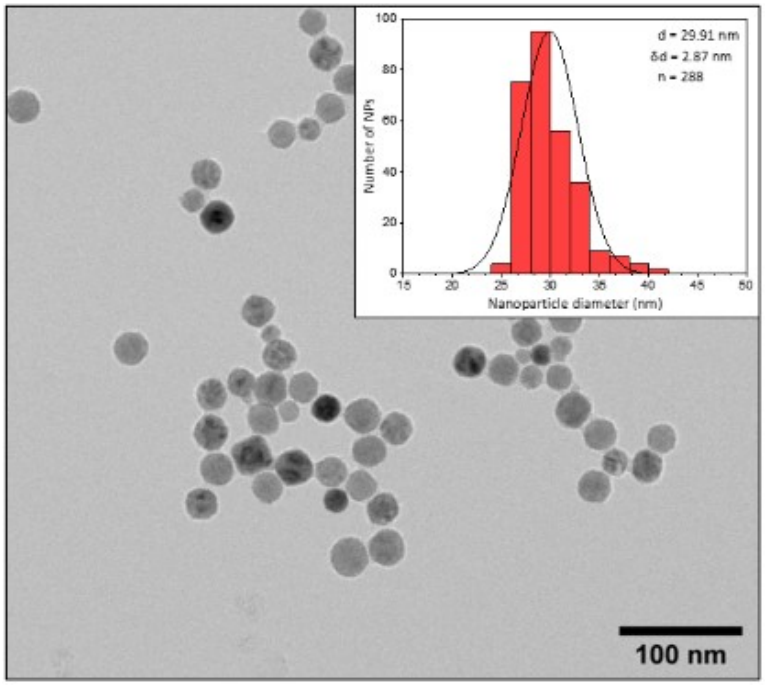

Figure 1~~9~~5S: Iron Oxide NPs stabilized by PMDA

5. Characterization of polymers

Unfunctionalized PMA - poly(isobutylene -alt-maleic anhydride)

The IR spectra of PMA revealed the presence of succinic anhydride. Two well-resolved bands at 1849 and 1770 cm^{-1} assigned to stretching vibrations (symmetric and asymmetric, respectively) for the anhydride in the polymer backbone. The band observed at 1075 cm^{-1} is assigned to bending of the C-O bond of anhydride rings.

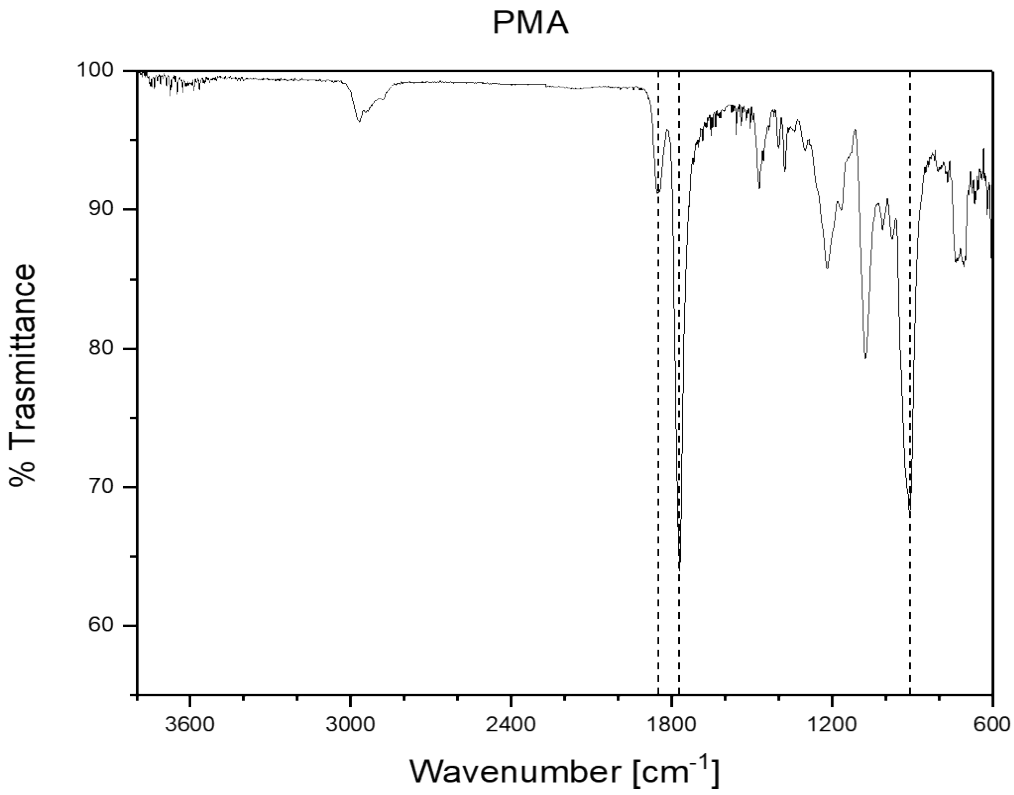

Figure ~~20~~16S: IR spectra of unfunctionalized PMA. Two well-resolved bands at 1849 and 1770 cm^{-1} are assigned the anhydride

PCP - poly[isobutene alt maleic anhydride] grafted with both 2-pyridylthio cysteamine and 750 Da PEG

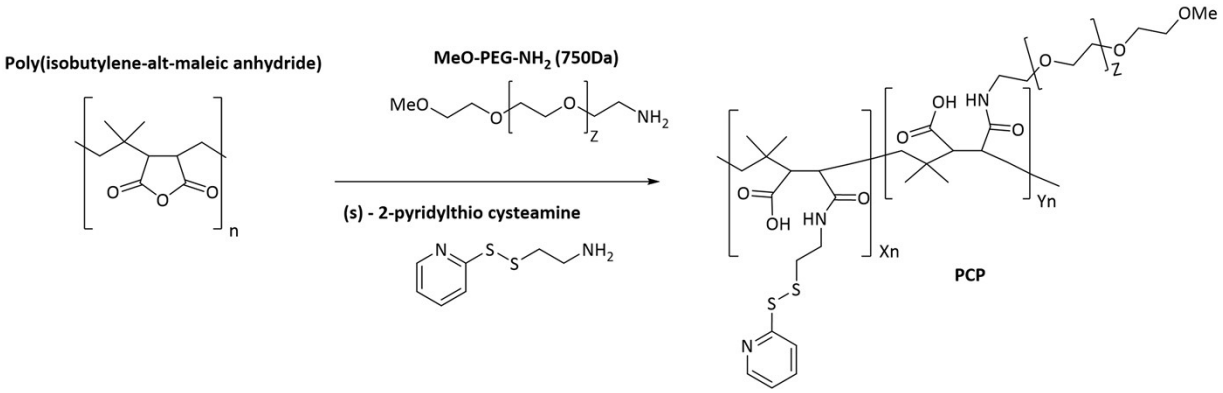

Figure 17~~21~~S: synthesis of PCP

The IR spectra of PCP shows a drop in anhydride absorption (1777 cm^{-1}) and increase in absorption related to amide bonds (1574 cm^{-1}) indicating the success of the reaction. Peaks

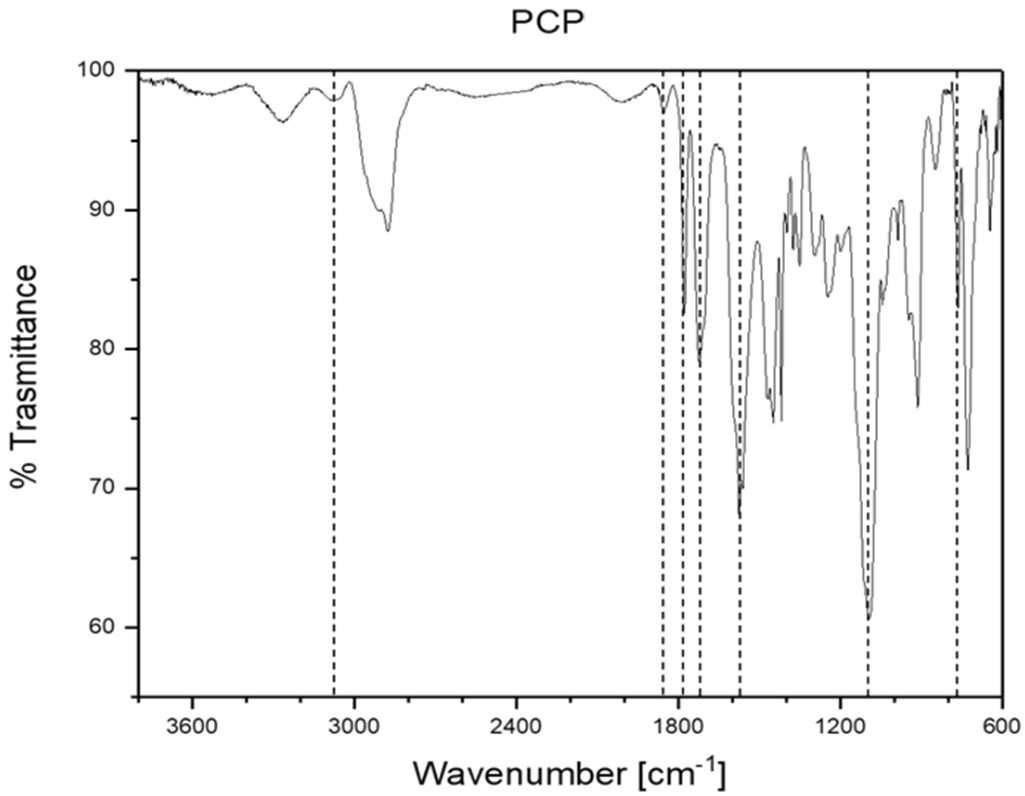

related to PEG and 2-pyridiylthio cysteamine are visible.

Figure ~~21~~82S: The IR spectra of PCP revealed the presence of PEG and 2-pyridiylthio cysteamine conjugated to the backbone of poly(isobutylene -alt-maleic anhydride). Two well-resolved bands at 1850 and 1777 cm^{-1} assigned to stretching vibrations for the residual anhydride in the polymer backbone. The bands observed at 3070 and 764 cm^{-1} demonstrate the presence of 2-

pyridiylthio cysteamine, the first vibration can be attributed to stretching of sp2 C-H and the second one to the bending mode of C-H in substituted aromatic ring. A sharp peak at 1091 cm^{-1} is typical of stretching vibration for C-O ether attributable to the PEG chains. The peaks that show the monomers are 1723 and 1574 cm^{-1} where the first one is due to the stretching- of C=O for amide and carboxylic acid, the second vibration is assigned to the bending of N-H in amide II.

^{1}H NMR characterization of PCP further validated the success of the reaction and allow to estimate the individual degree of functionalization for PEG and 2-pyridylthiol cysteamine (9-10 and 14 per PMA chain).[1]

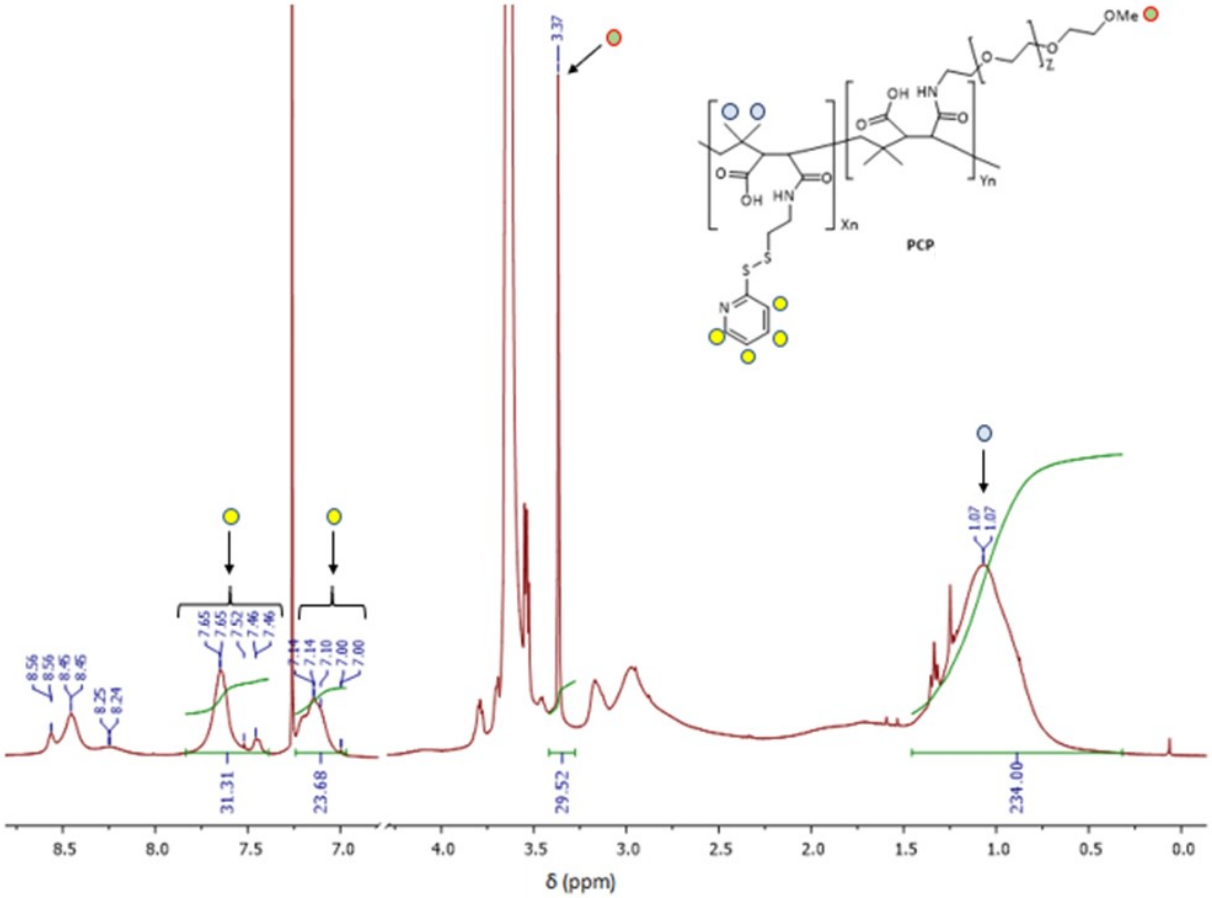

Figure ~~21~~~~3~~S: 1H-NMR spectrum PCP obtained in $CDCl_3$. The spectrum shows peaks between 7.0 and 8.5 ppm, characteristic of the protons in the 2-pyridylthiol ring. The sharp peaks at 3.63 ppm and 3.37 ppm attributed to the protons in the PEG chains and the terminal methyl group, respectively. The broad peak around 1 ppm is assigned to the protons of the methyl groups in the polymer chain. The degree of functionalization was obtained integrating the 4 protons of the 2-pyridylthiol ring (56.36 H), the 3 protons of the terminal methoxy group of the PEG chains (29.52 H) and the protons of the two methyl group in the monomeric units of polymer backbone (234.00 H). For PCP, we estimated ~14 2-pyridiylthio cysteamine and 9~10 PEG per polymer chain. The value for 2-pyridiylthio cysteamine confirm similar data obtained by the UV-Vis (data not shown).

.

PDP - poly[isobutene alt maleic anhydride] grafted with both dopamine and 750 Da PEG

Again, the IR spectra shows the reaction of the anhydride and formation of amide bonds. Peaks related to PEG and dopamine are also visible.

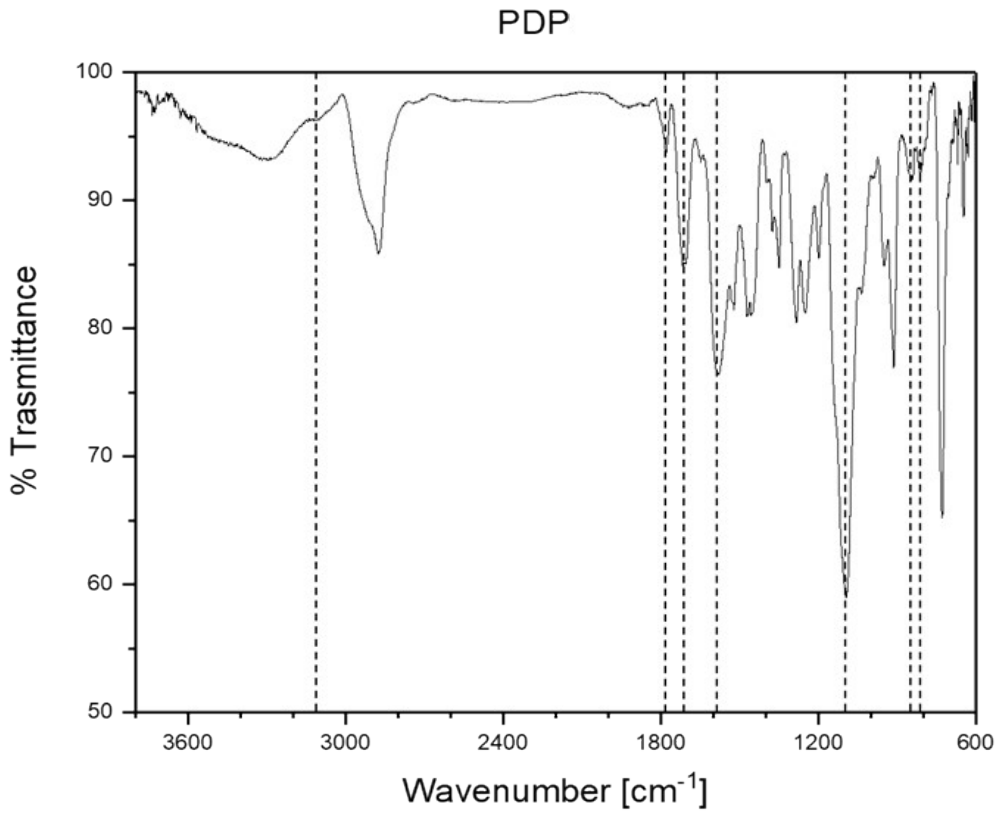

Figure 204S: The IR spectra of PDP revealed the presence of PEG and dopamine conjugated to the backbone of poly(isobutylene -alt-maleic anhydride). The peak at 1779 cm^{-1} is due to the starching vibration of C=O showing the presence of unreacted anhydride. The presence of dopamine can be demonstrated by the peaks at 3090 and 848-813 cm^{-1}, the first vibration attributed to stretching of sp^2 C-H and the second one to the bending modes of C-H in 1,2,4-trisubstituted benzene derivative. The sharp peak at 1094 cm^{-1} is assigned to the stretching vibration for C-O in the PEG chains. The peaks show the monomers are 1716 and 1580 cm^{-1} where the first one is due to the stretching of C=O for amide and carboxylic acid, the second vibration is assigned to the bending of N-H in amide II.

^{1}H NMR characterization of PDP further validated the success of the reaction and allow to estimate the individual degree of functionalization for PEG and dopamine (11 and 17-18 per PMA chain).[2]

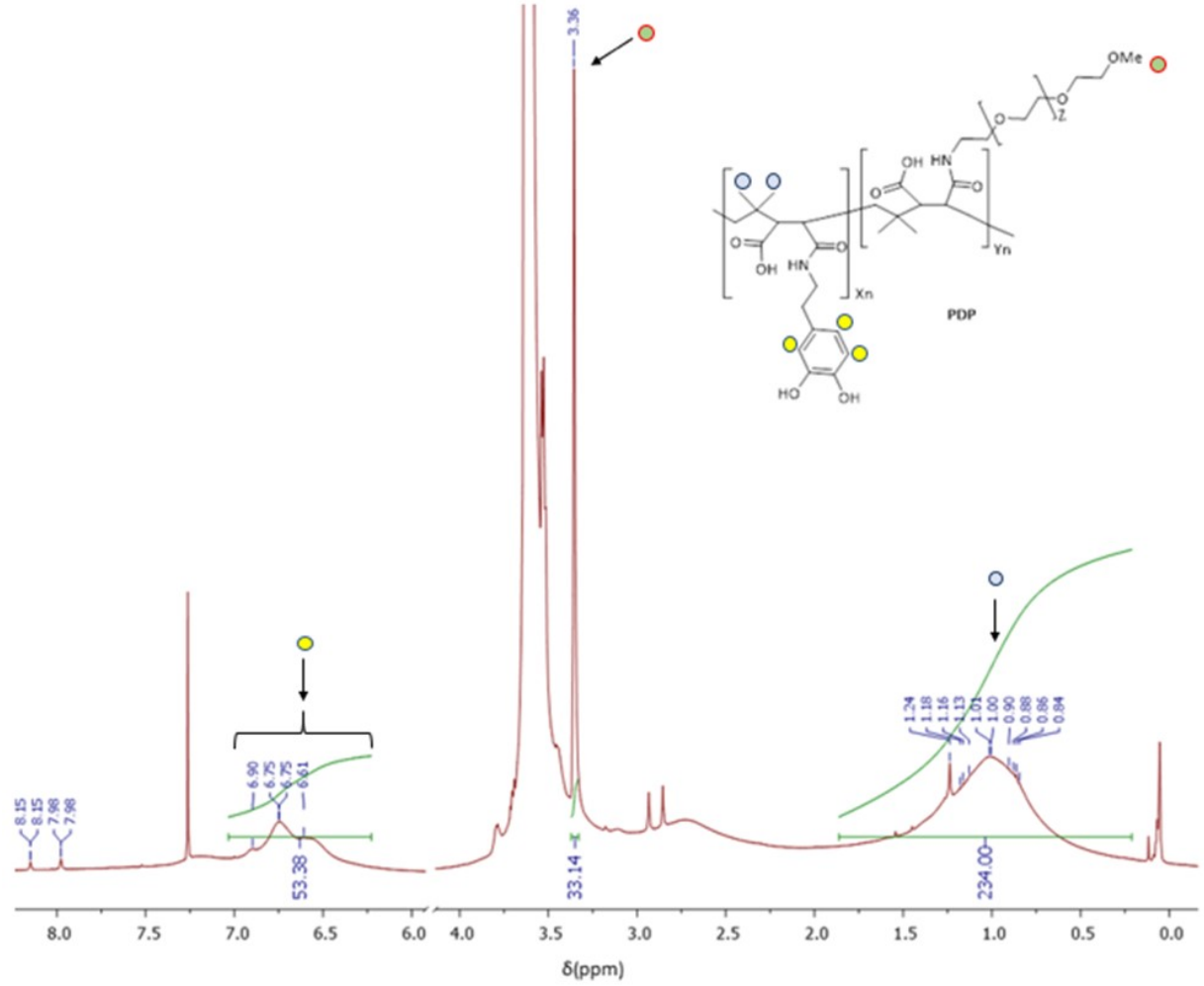

Figure 2~~1~~5S: 1H NMR characterization of PDP in $CDCl_3$. The spectrum shows peaks in region between 6.0 and 7.0 ppm, characteristic of the protons in the catechol ring. The sharp peaks at 3.62 ppm and 3.36 ppm attributed to the protons in the PEG chains and the terminal methyl group, respectively. The broad peak around 1 ppm is assigned to the protons of the methyl groups in the polymer chain. The degree of functionalization was obtained integrating the 3 protons of the catechol (53.38 H), the 3 protons of the terminal methoxy group of the PEG chains (33.14 H) and the protons of the two methyl group in the monomeric units of polymer backbone (234.00 H). For PDP750, we estimated 17~18 dopamine and ~11 PEG per polymer chain. These values confirm the data about the degree of dopamine functionalization obtained by the UV-Vis (data not shown).

6. Ligand affinity calculation using Density Functional Theory

The relative affinities of a series of ligands to both Au(100) and Au(111) facets have been calculated with Density Functional Theory (DFT) calculations. Each ligand constitutes the monomeric unit, part of a specific multidentate surfactant, that is predicted to directly bind to gold NPs. This monomeric unit has been modelled as reported in Figure 2~~2~~6S. As for Au surfaces, we used two alternative approaches for modelling, as reported in the Material and Methods section. In particular, we used both a finite-sized three-layers nanocluster derived from bulk gold (to give Au(100) and Au(111) models, Figure 2~~3~~7S) or from a 4 nm nanoparticle (to give AuNP (100) and AuNP(111) models, Figure 2~~3~~7S, B), all cleaved along the desired plane.

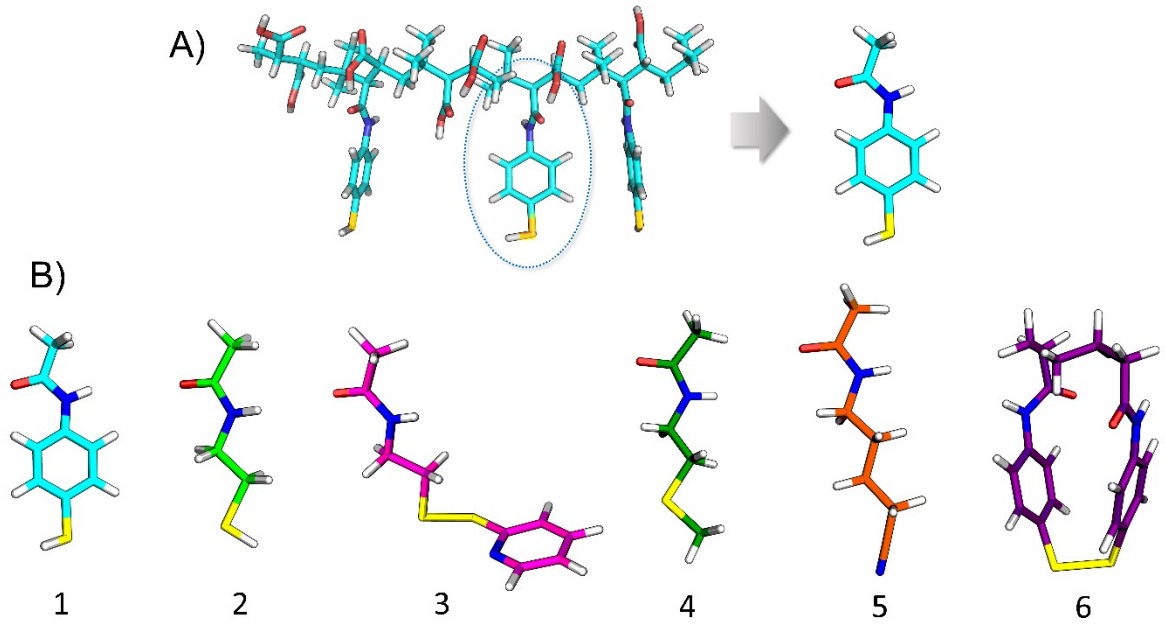

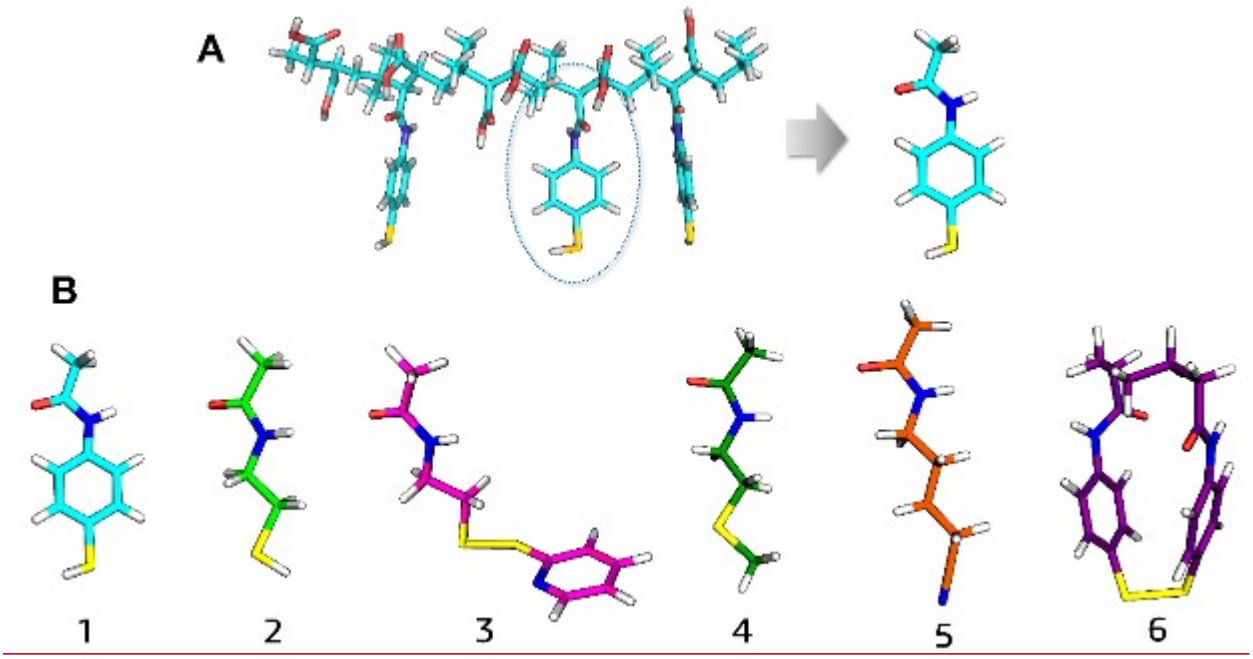

*Figure 2~~2~~6S: A) modelling approach for the thiol moiety of multidentate surfactants. B) PBE-D3 optimized structures of the ligands **1**-**6** computationally tested. 1: aminothiophenol. 2: cysteamine. 3: 2-pyridylthio cysteamine. 4: 2-(methylthio)ethylamine. 5: 5-aminopentanenitrile. 6: an oxidized aminothiophenol dimer.*

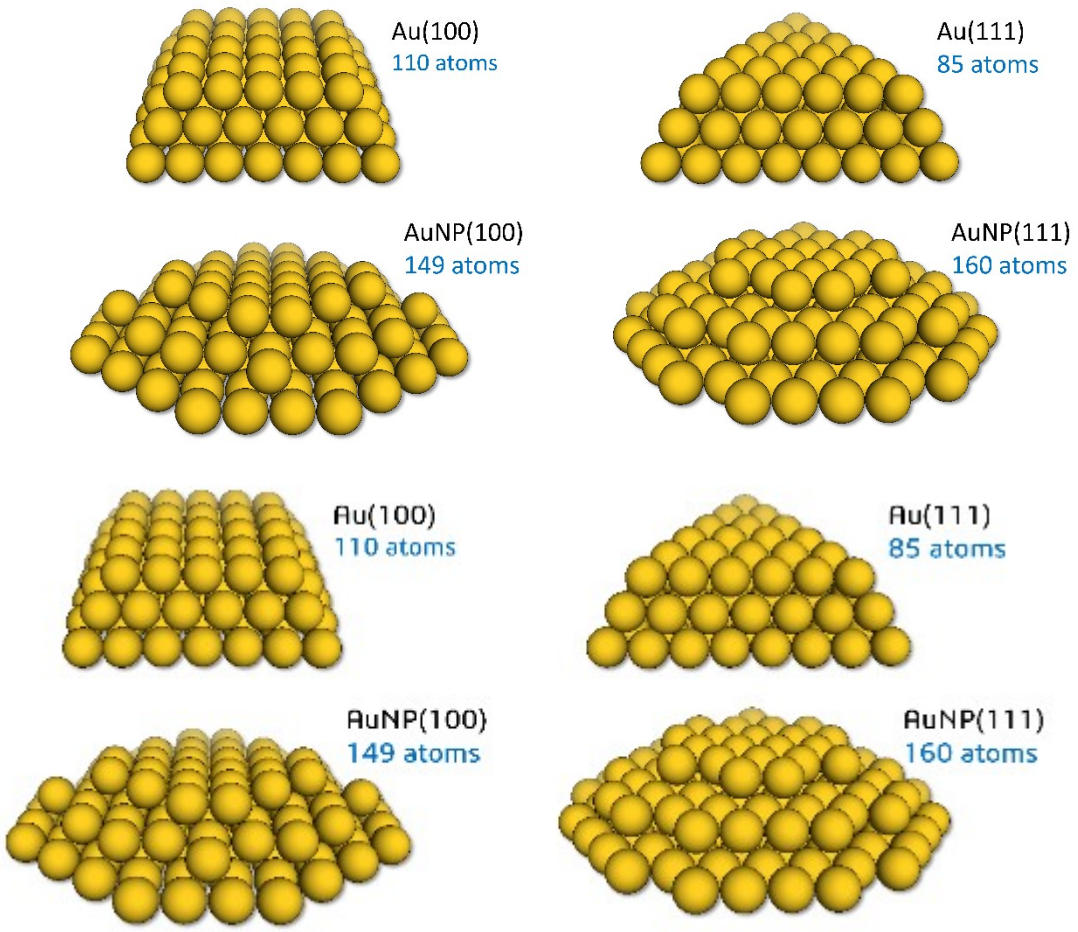

Figure ~~27~~S~~23~~S: Structure of the Au surfaces models adopted in the present investigations.

We first tested ligand binding modes of thiols **1** and **2** to the Au(100) and Au(111) models. The main results obtained for ligand **1** binding to both Au(100) and Au(111) facets are reported in Figure 2~~8~~4S. Essentially, three physisorption modes have been predicted, independently from the facet packing. Two out of three imply an almost perpendicular ligand disposition with respect to the surface normal, with an Au-(SH)-C angle approximating 180° (see A, B, D and E, Figure 24~~8~~S). In particular, structure: A corresponds to ligand physisorption at the hollow site of Au(100); B to the bridge site of Au(100); D to the *fcc* or hcp site of Au(111) and E to the bridge site of Au(111)). The third Au-S interaction mode involves Au(100) or Au(111) on-top sites and entails a decrease of tilt angle Au-(SH)-C, which gets close to 90° (see C and F, Figure 24~~8~~S). Since dispersion forces are assumed to be the predominant contribution to the gold-thiol interaction,[3,4] we used two different levels of theory (PBE-D3 and B97-D) which account for dispersions but using two alternative theoretical schemes (see the Material and Methods section). However, results obtained with the two functionals are very similar, both in terms of energetic and geometric values. In agreement with literature,[5] binding energies obtained for

Au(111) are generally smaller than the ones predicted for Au(100), because of the tighter surface packing of the former.

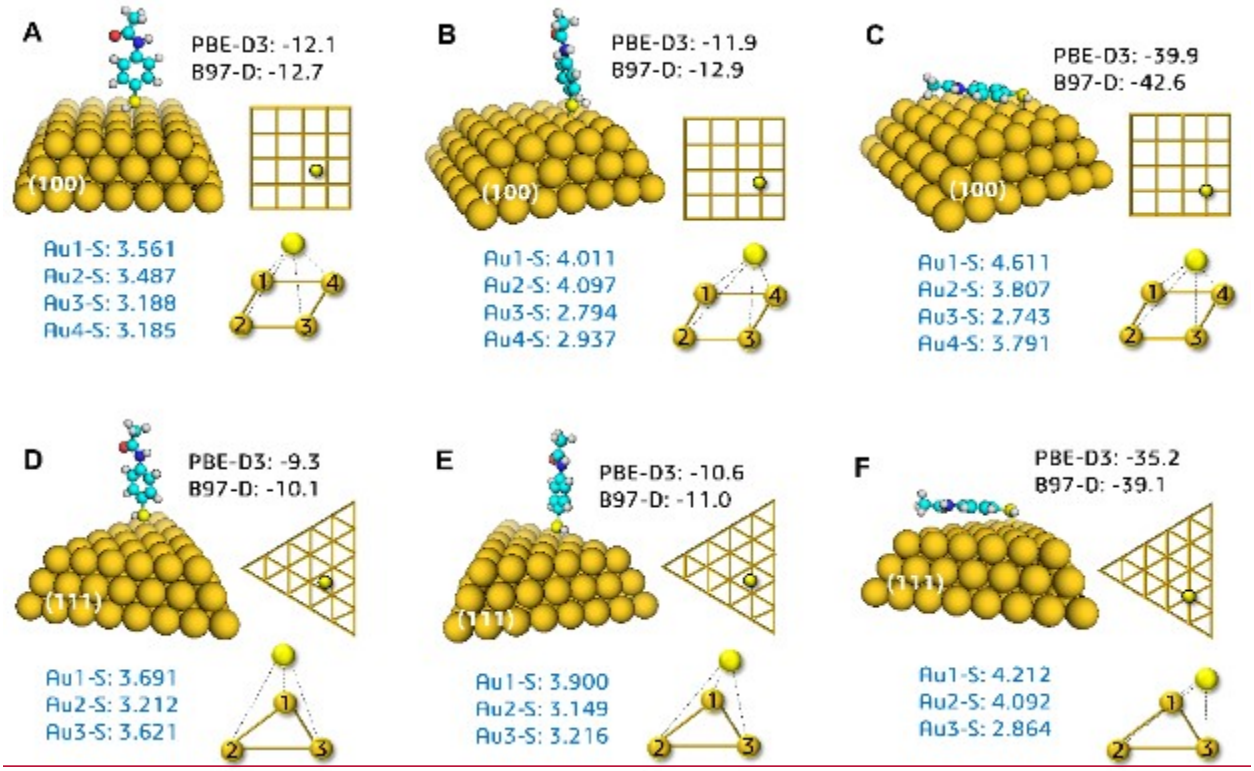

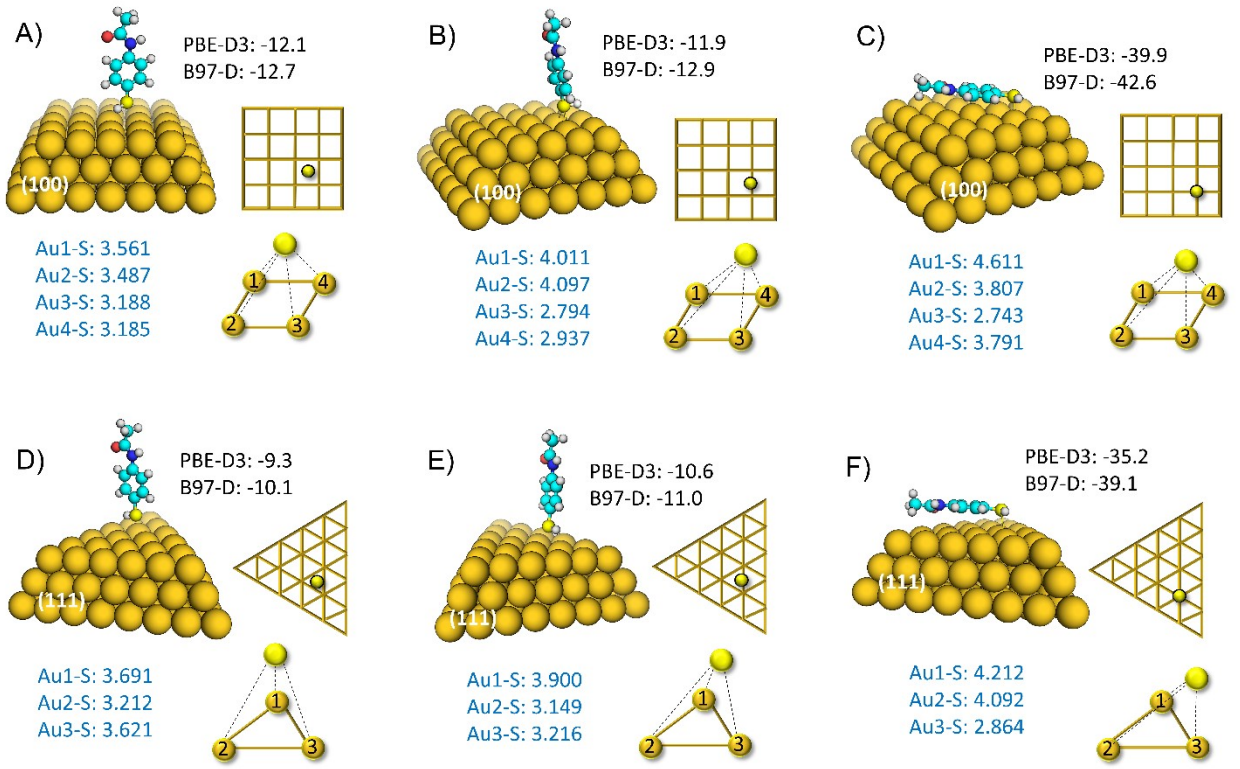

*Figure 2~~4~~8S: In-solvent optimized structures obtained at the PBE-D3 level of the most relevant physisorption modes of **1** to both Au(100) and Au(111) nanoclusters. Binding energies obtained at the PBE-D3 and at the B97-D levels of theory are reported (black values, kcal/mol), together with the main geometrical parameters of PBE-D3 optimized geometries (blue values, Å). Each Au-ligand adduct is accompanied by a schematic top-view representation, indicating the positioning of the S atom on gold surfaces.*

Structures A and B (or D and E for slab(111)) are isoenergetic, so, as expected, there is not a preferential site for "vertical" physisorption. Binding mode C (and F as well), maximizes the number of Van der Waals contacts between the ligand and gold and it is significantly more stable than any other characterized binding mode. The calculated binding energies (in the range -35-40 kcal/mol) are in nice agreement with previous DFT calculations on aromatic thiol binding to gold surfaces.[3] This "horizontal" binding mode of thiols and thioethers and disulfides generally dominates the early phases of self-assembled monolayers (SAMs) formation[6] and is preferred for low surface coverage,[7] so its calculated high stability is reasonable in light of the absence of inter-ligand interactions in our model and of explicit solvent molecules.

Analogous considerations can be made for **2**, where the phenyl ring is substituted by an ethyl group. In Figure 2~~5~~9S, we report only long range vertical physisorption in proximity of slab(100) hollow site (A) and slab(111) fcc site (D), but equal energies have been obtained considering all the other possibilities. The increased ligand flexibility with respect to **1** allows an additional binding mode, see structures B and E. Here the tilt Au-S-C angle is around 90°, but the rest of the ligand is not lying down on the surface. Again, PBE-D3 and B97-D energies are very similar. For this reason, we will discuss hereafter only binding energies obtained at the PBE-D3 level.

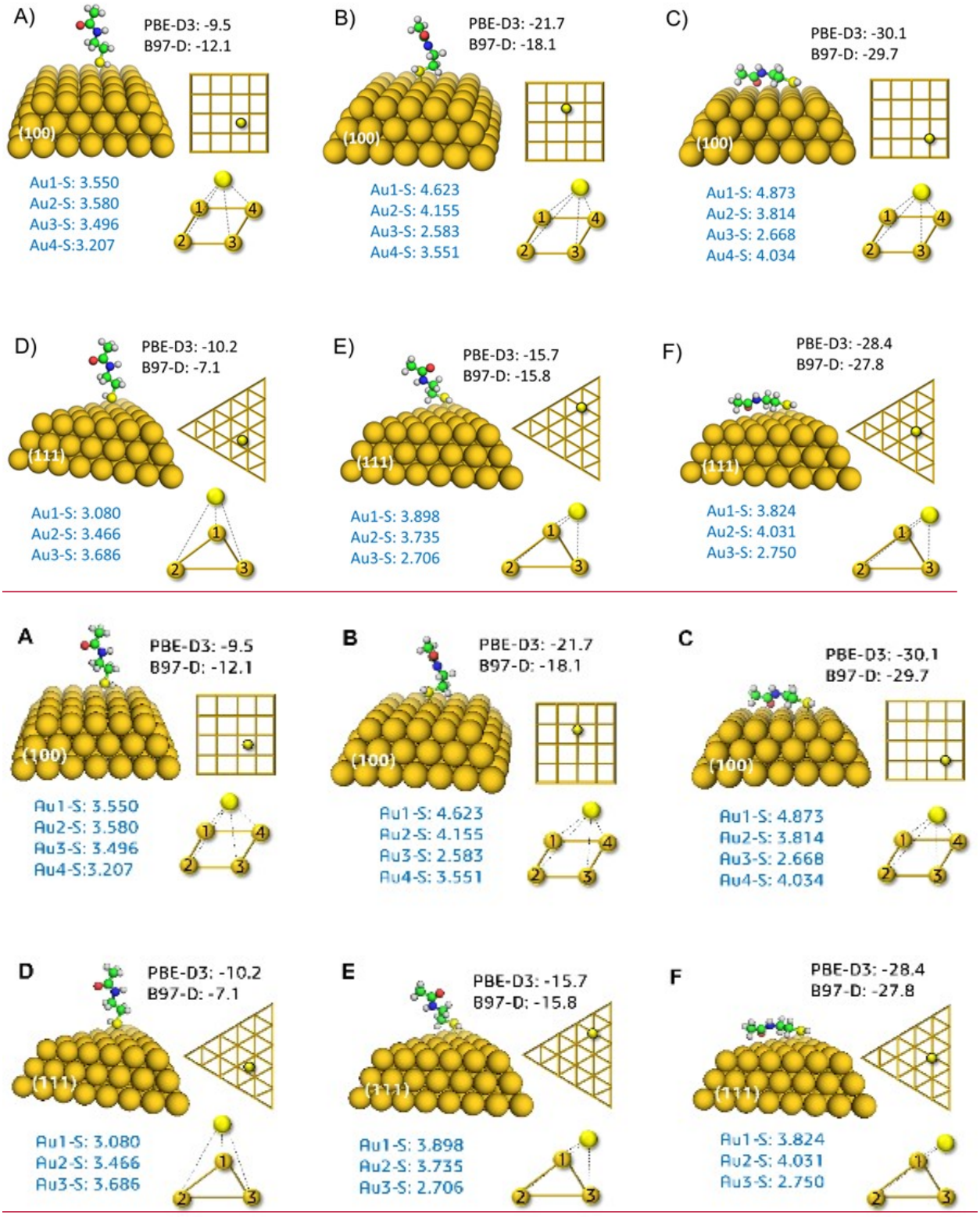

*Figure 2~~59~~S: In-solvent optimized structures obtained at the PBE-D3 level of the most relevant physisorption modes of **2** to both Au(100) and Au(111) nanoclusters. Binding energies obtained at the PBE-D3 and at the B97-D levels of theory are reported*

(black values, kcal/mol), together with the main geometrical parameters of PBE-D3 optimized geometries (blue values, Å). Each Au-ligand adduct is accompanied by a schematic top-view representation, indicating the positioning of the S atom on gold surfaces.

Independently from the nature of the organic portion of the thiol ligand, the calculated energy difference between "vertical" and "horizontal" binding modes is very huge (~30 kcal/mol for **1** and ~20 kcal/mol for **2**). However, despite this energy difference could be realistic if considering a single ligand approaching to gold surface, in the case of nanoparticle coverage by multiple chains of multidentate surfactants, the high stabilization of a "horizontal" binding mode could be an artifact. Indeed, in our computational model we don't consider inter-chains interactions nor the effect of explicit solvent molecules. For these reasons, hereafter, when comparing different ligands, we will discuss only binding energy values obtained for those binding modes with a low van der Waals contribution deriving from the direct interaction between gold surface and the organic portion of the ligands.

A similar systematic approach for binding modes search has been performed for the other ligands of the series, **3**-**6**. Because of the increased ligands size with respect to **1** and **2**, a larger Au slab has been used and chosen in order to account for the curvature of the NP (see Material and Methods). The most relevant structures of each ligand bound to AuNP(100), including also ones of **1** and **2**, are reported in Figure 26~~30~~S. Similar structures and binding energies trend have been obtained for AuNP(111). Calculated PBE-D3 binding energy for **1** and **2** to AuNP(100) (considering the lying down binding mode) are -40.1 kcal/mol and -29.4 kcal/mol, respectively, in line with binding energies to Au(100) (see above).

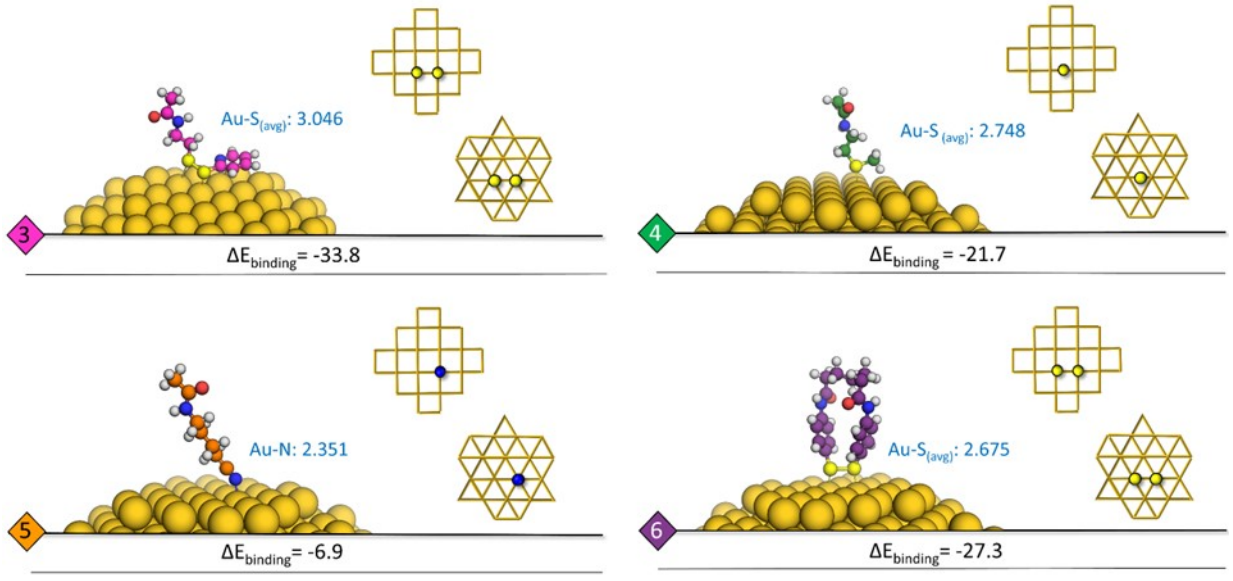

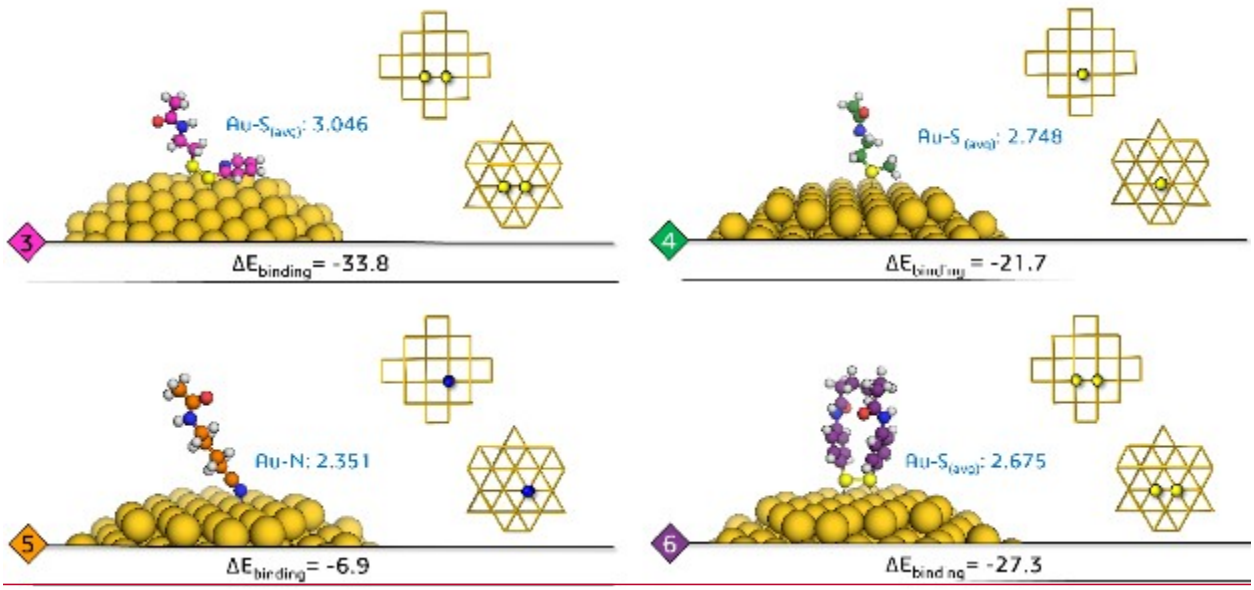

*Figure ~~3~~2~~60~~S: In-solvent optimized structures obtained at the PBE-D3 level of the most relevant physisorption modes of **3-6** to AuNP(100) and corresponding relevant geometrical parameters (blue values, Å). Binding energies obtained at the PBE-D3 are reported as average value obtained for the AuNP(100) and AuNP(111) facets (black values, kcal/mol). Each Au-ligand adduct is accompanied by a schematic top-view representation, indicating the positioning of the S or N atom on gold (111) and (100) surfaces.*

Ligand **3** is the one undergoing the strongest physisorption to gold. Here the S-S bond has been preserved and not homolytically splitted since it has been shown very recently that disulfides are presumably physisorbed and not chemisorbed on gold.[8] In any case, the chemisorption of disulfides should be significantly slower with respect to the one of thiols.[9]

Similar consideration can be made for **6**. Its binding energy is almost double the one for **1** since there are two S atoms, instead of one, interacting with the surface. But, because of the lack of an aromatic portion interacting with gold, binding is a little disfavored with respect to the one of **3**.

Ligand **5** is only physisorbed on the surface, as the nitrile group preserves its planarity, and it gives the weakest interaction with gold. This probably results from the lower Au-affinity of N compared to S or from the fact the CN moiety creates a spacer group, separating the organic portion from Au surface and thus limiting the vdW contacts.

The binding modes of **4** are very similar to the ones of **2**, but binding is more favored for **4**. This is because the replacement of -H with -CH_3, switching from thiol to thioether, creates additional favorable dispersive contacts with the surface. Anyway, it has been observed that thiols have a higher affinity for gold than thioether.[10] This can be ascribed to the fact that a certain percentage of -SH units can be homolytically broken, leading to a complete thiol chemisorption which entails the formation of a strong Au-S covalent bond (see below). This process, which in the past has been theoretically predicted to be strongly energetically downhill starting from physisorbed species,[3,11] has been also very recently experimentally confirmed for thiols.[8]

Chemisorbed structures on AuNP(100) of **1** are collected in Figure 27~~31~~S, together with main geometrical parameters and binding energies.

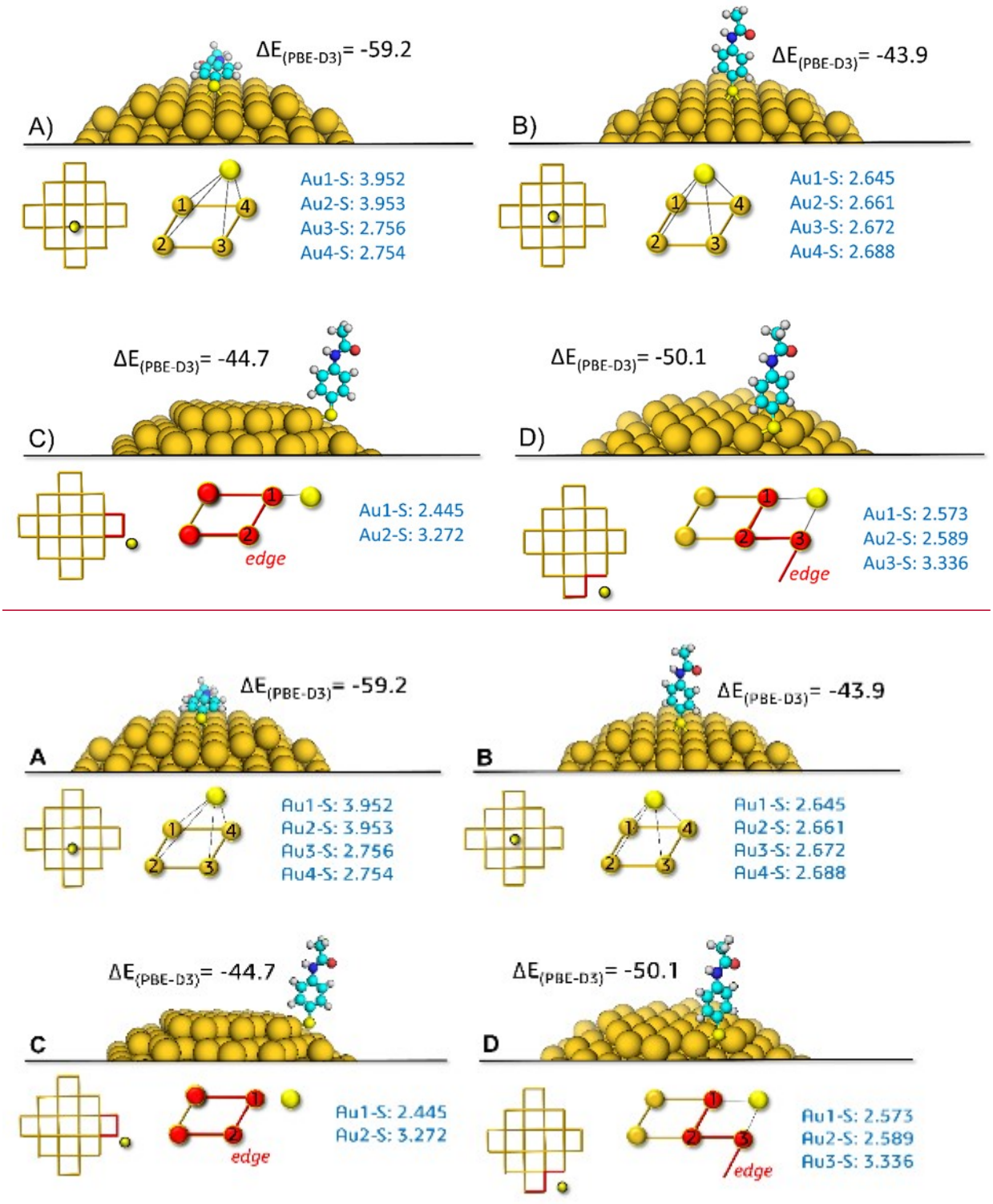

*Figure ~~3~~27~~1~~S: In-solvent optimized structures obtained at the PBE-D3 level of the most relevant chemisorption modes of **1** to AuNP(100) and corresponding relevant geometrical parameters (blue values, Å). Binding energies, calculated as average*

*chemical adsorption energies of **1** to AuNP(100) and AuNP(111), obtained at the PBE-D3, are reported (black values, kcal/mol). Each Au-ligand adduct is accompanied by a schematic top-view representation, indicating the positioning of the S atom on gold (100) surface.*

Among the characterized two binding modes to the Au(100) facet, A is the most stable one. It corresponds, again, to **1** lying-down binding mode, dramatically more stable than vertically bound ligands (such as B) because of the strong contribution of dispersions. Here the S atom is in bridging position between two Au atoms, in line with previous works.[3] In B, instead, a "sp" sulfur atom interacts with four Au centers.

If chemisorption involves non-facets gold atoms, such as edge ones (see C, with S bound to a single edge Au and D with S bound to two edge Au atoms in a bridging fashion), binding processes that do not involve a parallel stacking of ph π-system and gold surfaces are lowered in energy. This is in line with the expectation that chemisorption should be triggered at non-facets centers (defects, adatoms, edges, corners) or on irregular NP surfaces.[12]

For AuNP(111) the preferred binding mode for **1** is in bridge position, with the S atom slightly bent towards the *fcc* site, as already reported for other thiols.[13] The overall picture is analogous to the one described for AuNP(100). In the B-like more stable structure the ligand occupies the *fcc* site. Average Au-S distances are shortened with respect to physisorbed structures (Figure 23~~31~~S).

	1	**2**	**3**	**4**	**5**	**6**
Physisorption	-11.3	-18.7	-33.8	-21.7	-7.5	-27.2
Chemisorption	-43.9	-44.3				

*Table 1S: summary of physisorption and chemisorption energies (kcal/mol) of **1**-**6**, calculated as average binding energies to Au(100) and Au(111) facets at the PBE-D3 level.*

7.

7.

7.

7.

7.

7.

7.

7.

7.

7.

7.

7.

7.

7.

7.

7.

7. References

[1] L. Liu, L. Wu, J. Tan, L. Wang, Q. Liu, P. Liu, L. Liu, *Polym. Chem.* **2015**, *6*, 3934.

[2] W. Wang, G. Palui, X. Ji, F. Aldeek, H. Mattoussi, in *Colloid. Nanoparticles Biomed. Appl. IX* (Eds: W.J. Parak, M. Osinski, K.I. Yamamoto), International Society For Optics And Photonics, **2014**, p. 89550B.

[3] S. Miranda-Rojas, A. Muñoz-Castro, R. Arratia-Pérez, F. Mendizábal, *Phys. Chem. Chem. Phys.* **2013**, *15*, 20363.

[4] J. R. Reimers, M. J. Ford, S. M. Marcuccio, J. Ulstrup, N. S. Hush, *Nat. Rev. Chem.* **2017**, *1*, DOI 10.1038/s41570-017-0017.

[5] H. Al-Johani, E. Abou-Hamad, A. Jedidi, C. M. Widdifield, J. Viger-Gravel, S. S. Sangaru, D. Gajan, D. H. Anjum, S. Ould-Chikh, M. N. Hedhili, A. Gurinov, M. J. Kelly, M. El Eter, L. Cavallo, L. Emsley, J. M. Basset, *Nat. Chem.* **2017**, *9*, 890.

[6] C. Vericat, M. E. Vela, G. Benitez, P. Carro, R. C. Salvarezza, *Chem. Soc. Rev.* **2010**, *39*, 1805.

[7] H. Häkkinen, *Nat. Chem.* **2012**, *4*, 443.

[8] M. S. Inkpen, Z. –F Liu, H. Li, L. M. Campos, J. B. Neaton, L. Venkataraman, *Nat. Chem.* **2019**, *11*, 351.

[9] N. Garg, J. M. Friedman, T. R. Lee, *Langmuir* **2000**, *16*, 4266.

[10] T. Weidner, N. Ballav, U. Siemeling, D. Troegel, T. Walter, R. Tacke, D. G. Castner, M. Zharnikov, *J. Phys. Chem. C* **2009**, *113*, 19609.

[11] H. Grönbeck, A. Curioni, W. Andreoni, *J. Am. Chem. Soc.* **2000**, *122*, 3839.

[12] C. Vericat, G. A. Benitez, D. E. Grumelli, M. E. Vela, R. C. Salvarezza, *J. Phys. Condens. Matter* **2008**, *20*, DOI 10.1088/0953-8984/20/18/184004.

[13] J. Nara, S. Higai, Y. Morikawa, T. Ohno, *J. Chem. Phys.* **2004**, *120*, 6705.